THE JOURNAL OF BIOLOGICAL CHEMISTRY VOL. 287, NO. 14, pp. 11498–11515, March 30, 2012

EMILIN-3, Peculiar Member of Elastin Microfibril Interface-located Protein (EMILIN) Family, Has Distinct Expression Pattern, Forms Oligomeric Assemblies, and Serves as Transforming Growth Factor β (TGF-β) Antagonist*[S]

Received for publication, September 12, 2011, and in revised form, January 23, 2012 Published, JBC Papers in Press, February 10, 2012, DOI 10.1074/jbc.M111.303578

Alvise Schiavinato[‡], Ann-Kathrin A. Becker[§], Miriam Zanetti[‡], Diana Corallo[‡], Martina Milanetto[‡], Dario Bizzotto[‡], Giorgio Bressan[‡], Marija Guljelmovic[‡], Mats Paulsson[§¶‖], Raimund Wagener[§¶], Paola Braghetta[‡], and Paolo Bonaldo[‡1]

From the [‡]Department of Biomedical Sciences, University of Padova, I-35121 Padova, Italy and [§]Center for Biochemistry, Medical Faculty, [¶]Center for Molecular Medicine Cologne (CMMC), and [‖]Cologne Excellence Cluster on Cellular Stress Responses in Aging-Associated Diseases (CECAD), University of Cologne, D-50931 Cologne, Germany

Background: EMILIN-3 is the least characterized member of the EMILIN/Multimerin family.
Results: EMILIN-3 forms homotrimers and higher order oligomers, binds heparin, has a dynamic expression during development and a restricted distribution in adult tissues, and serves as a pro-TGF-β antagonist.
Conclusion: The structure and expression of EMILIN-3 are different from other EMILINs/Multimerins.
Significance: EMILIN-3, a TGF-β antagonist, is likely to be an important regulator during development of several tissues.

EMILIN-3 is a glycoprotein of the extracellular matrix belonging to a family that contains a characteristic N-terminal cysteine-rich EMI domain. Currently, EMILIN-3 is the least characterized member of the elastin microfibril interface-located protein (EMILIN)/Multimerin family. Using RNA, immunohistochemical, and protein chemistry approaches, we carried out a detailed characterization of the expression and biochemical properties of EMILIN-3 in mouse. During embryonic and postnatal development, EMILIN-3 showed a peculiar and dynamic pattern of gene expression and protein distribution. EMILIN-3 mRNA was first detected at E8.5–E9.5 in the tail bud and in the primitive gut, and at later stages it became abundant in the developing gonads and osteogenic mesenchyme. Interestingly and in contrast to other EMILIN/Multimerin genes, EMILIN-3 was not found in the cardiovascular system. Despite the absence of the globular C1q domain, immunoprecipitation and Western blot analyses demonstrated that EMILIN-3 forms disulfide-bonded homotrimers and higher order oligomers. Circular dichroism spectroscopy indicated that the most C-terminal part of EMILIN-3 has a substantial α-helical content and forms coiled coil structures involved in EMILIN-3 homo-oligomerization. Transfection experiments with recombinant constructs showed that the EMI domain contributes to the higher order self-assembly but was dispensable for homotrimer formation. EMILIN-3 was found to bind heparin with high affinity, a property mediated by the EMI domain, thus revealing a new function for this domain that may contribute to the interaction of EMILIN-3 with other extracellular matrix and/or cell surface molecules. Finally, *in vitro* experiments showed that EMILIN-3 is able to function as an extracellular regulator of the activity of TGF-β ligands.

EMILINs[2] belong to a family of secreted glycoproteins sharing some structural features and a unique N-terminal cysteine-rich region, the EMI domain. The term EMILIN was first coined to describe an elastin microfibril interface-located protein (1) (now called EMILIN-1). In mammals, the "EMILIN/Multimerin" family includes five genes coding for EMILIN-1, EMILIN-2, EMILIN-3, Multimerin-1, and Multimerin-2 (2).[3] Besides the common presence of the EMI domain, these proteins contain a long region predicted to form coiled coil structures and a globular C1q (gC1q) domain at their C-terminal end (3–6). EMILIN-3 is the only protein of the family that lacks the gC1q domain in its C-terminal region (see also Fig. 1*A*) (2, 7, 8).

The EMI domain spans ~80 amino acids and is characterized by the presence of highly conserved cysteine residues located at regular positions (9). This domain is rather unique as (i) it is always located in a single copy at the N-terminal portion of the mature protein and (ii) it encodes for seven cysteine residues, whereas the majority of cysteine-rich domains contain either six or eight cysteine residues. It has been demonstrated that the EMI domain of EMILIN-1 binds pro-TGF-β1, thereby preventing its proteolytic processing into the mature and active cytokine (10). The gC1q domain was shown to be essential for the cell adhesion properties of EMILIN-1, and it was proposed that

* This work was supported by the University of Padova (Grant CPDA075559), the Italian Ministry of University and Research (Progetti di Ricerca di Interesse Nazionale), and the German Research Council (Deutsche Forschungsgemeinschaft Grants WA1338/2-6 and SFB 829).
[S] This article contains supplemental Figs. S1–S8.
[1] To whom correspondence should be addressed: Dept. of Biomedical Sciences, University of Padova, Viale G. Colombo 3, I-35121 Padova, Italy. Tel.: 39-049-827-6084; Fax: 39-049-827-6079; E-mail: bonaldo@bio.unipd.it.

[2] The abbreviations used are: EMILIN, elastin microfibril interface-located protein; ECM, extracellular matrix; GdnHCl, guanidine hydrochloride; gC1q, globular C1q; RIPA, radioimmune precipitation assay.
[3] Several names are used for the members of the EMILIN/Multimerin family in the literature. In this study, we adopted the current approved nomenclature (see also HUGO Gene Nomenclature Committee). Previous names include gp115 and EMILIN (for EMILIN-1), Basilin and FOAP-10 (for EMILIN-2), EMILIN-5 and EMILIN-T (for EMILIN-3), EMILIN-4 and Multimerin (for Multimerin-1), and EndoGlyx-1 and EMILIN-3 (for Multimerin-2).

this domain is involved in the supramolecular organization and assembly of EMILIN-1 into multimers (11, 12). EMILIN-1 and Multimerin-1 were shown to multimerize, forming disulfide-linked trimers and larger complexes reaching a size of several million daltons (11, 13). EMILINs/Multimerins contain various regions endowed with oligomerization capability, such as the gC1q and EMI domains, collagen repeats, and long regions potentially forming coiled coil structures. Although the effective formation of coiled coil structures in these proteins was never demonstrated until now, it was suggested that coiled coil stretches and the gC1q domain may be implicated in the oligomerization of EMILINs/Multimerins into higher order structures.

Previous studies have provided information on the expression pattern of some EMILIN/Multimerin genes during mouse development (2, 7, 14). As a general feature, different members of the EMILIN/Multimerin family show both overlapping and complementary expression patterns. Among them, EMILIN-1 displays the most abundant and broad expression (14). A common hallmark of mammalian EMILIN-1, EMILIN-2, Multimerin-1, and Multimerin-2 is their abundance throughout the cardiovascular system during both embryonic development and postnatal life (2, 7, 14). A study carried out in *Danio rerio* yielded information on the expression of EMILIN/Multimerin genes during fish development, confirming that the zebrafish orthologs coding for EMILIN-1, EMILIN-2, and Multimerin-2 are abundantly expressed in the cardiovascular system (15). Interestingly, zebrafish EMILIN-3 orthologs are not expressed in heart and vessels, and they display a peculiar expression in the developing notochord and in craniofacial cartilage primordia (15).

The *in vivo* biological functions of EMILINs/Multimerins are largely unknown, and thus far only the phenotype of EMILIN-1 knock-out mice has been characterized in detail. Mice deficient for EMILIN-1 show subtle structural alterations of the elastic fibers and of the cells in the wall of large blood vessels (16). Further studies revealed that EMILIN-1 knock-out mice are affected by arterial hypertension due to increased TGF-β signaling in the vascular wall, which is consistent with the finding that EMILIN-1 is a regulator of TGF-β processing and activation (10). Moreover, EMILIN-1 knock-out mice display defects in skin and in the lymphatic system (17, 18). *In vitro* and *in vivo* studies pointed at a role for EMILIN-2 as an extracellular regulator of apoptosis through binding of the tumor necrosis factor-related apoptosis-inducing ligand (TRAIL) receptors (19).

Thus far only a few data are available on EMILIN-3 expression and distribution, and the biochemical properties of this protein have not been investigated.[3] In a previous study aimed at identifying human genes associated with skeletal development, a gene designated "*EMILIN-5*" and coding for a deduced protein corresponding to EMILIN-3 was found to be expressed in some mesenchymal cells during *in vitro* induction of osteogenesis and in the perichondrium of developing limbs (8). Another study suggested that the gene for EMILIN-3 is expressed at sites of mesenchymal condensations during cartilage and bone formation (7). Here we present a detailed study of the expression of EMILIN-3 during mouse embryonic and postnatal development together with a characterization of the biochemical properties of the endogenous protein and its recombinant products.

EXPERIMENTAL PROCEDURES

RT-PCR—Total RNA was extracted from different organs of newborn and adult mice, mouse embryos, and cultured cells using TRIzol Reagent (Invitrogen) as recommended by the manufacturer. First strand cDNA synthesis was performed with 0.8 μg of total RNA using random hexanucleotides and SuperScript reverse transcriptase (Invitrogen). Amplification was carried out in 50-μl reaction mixtures containing 0.1–0.3 μg of cDNA, 10 mM Tris-HCl, pH 9.0, 50 mM KCl, 1.5 mM $MgCl_2$, 0.1% Triton X-100, 0.2 mM dNTPs, 25 pmol of each primer, and 2 units of *Taq* I polymerase (Promega). The optimal annealing conditions and number of cycles were determined to allow amplification of samples within the exponential phase of the PCR. After 25–35 amplification cycles, the reaction products were separated in 1% agarose gels. The following primers were used: murine EMILIN-3: 5′-ACA GCC CAG TGC CTC CCG TTA CA-3′ (forward) and 5′-CAG GGT GCC ATA TGC TTG CGA CA-3′ (reverse); reaction product, 487 bp; murine EMILIN-3L and -3S: 5′-CCC GTT ACA GCC TCT ACA CCA CC-3′ (forward) and 5′-CAG CCC ACG CAC CTC ATC TAA CA-3′ (reverse); reaction products, 696 (EMILIN-3L) or 555 bp (EMILIN-3S); murine eIF1A: 5′-AAG AAG TCT GAA GGC CTA TG-3′ (forward) and 5′-CAG AGA ACT TGG AAT GTA GC-3′ (reverse); reaction product, 170 bp; human EMILIN-3: 5′-CCA GGA CAC AGC CCA GAA ACT T-3′ (forward) and 5′-GGT GAT GTT CCC CGA GTT GG TG-3′ (reverse); reaction product, 330 bp; and human GAPDH: 5′-ACC CAC TCC TCC ACC TTT GAC G-3′ (forward) and 5′-CTC TCT TCC TCT TGT GCT CTT GC-3′ (reverse); reaction product, 186 bp.

Northern Blotting—Total RNA (15 μg) was extracted from newborn murine tissues with TRIzol Reagent, separated in 1% formaldehyde gels, transferred to nylon membranes (Hybond N, Amersham Biosciences), and hybridized at 42 °C with a ^{32}P-labeled 1.1-kb cDNA probe spanning the 3′-region of murine EMILIN-3 cDNA.

In Situ Hybridization—In situ hybridization on whole mouse embryos and sections was performed as described previously (14) using a digoxigenin-labeled antisense 2.3-kb riboprobe synthesized from murine EMILIN-3 full-length cDNA. Nonspecific hybridization was evaluated with the respective sense riboprobe.

Preparation of Recombinant Murine EMILIN-3 C-terminal Region—A cDNA construct coding for the C-terminal region of murine EMILIN-3 (EMILIN-CTR; amino acids 171–758) was generated by RT-PCR and cloned with 5′-terminal NheI and 3′-terminal BamHI restriction sites using oligonucleotide primers 5′-CAA TGC TAG CTG GAA GAA AAG GCC AAG GG-3′ (forward) and 5′-CAA TGG ATC CGT CAG CTC GCC CTG GCC G-3′ (reverse). The amplified PCR product was inserted into a modified pCEP-Pu vector containing an N-terminal BM-40 signal peptide (20) and a C-terminal One-STrEP-tag (IBA GmbH) downstream of the restriction sites. The recombinant plasmids were introduced into HEK293-EBNA cells (Invitrogen) using FuGENE 6 transfection reagents (Roche

Applied Science). Cells were selected with puromycin (1 mg/ml), and the recombinant protein was purified from serum-containing culture medium. After filtration and centrifugation for 1 h at 10,000 × *g*, the cell culture supernatants were applied to a Streptactin column (1.5 ml; IBA GmbH) and eluted with 2.5 mM desthiobiotin, 10 mM Tris-HCl, pH 8.0.

Preparation of Antibodies against Murine EMILIN-3—Purified recombinant EMILIN-3CTR was used for rabbit and guinea pig immunization. The obtained antisera were purified by affinity chromatography on a column with antigen coupled to CNBr-activated Sepharose (GE Healthcare). Specific antibodies were eluted with 0.1 M glycine, pH 2.5, and the eluate was neutralized with 1 M Tris-HCl, pH 8.8.

Immunohistochemistry—Frozen sections (7 μm) were prepared from 2-month-old mice, washed in PBS, and saturated with 10% goat serum (Sigma). Sections were incubated overnight with EMILIN-3 antibodies diluted 1:1000 in PBS supplemented with 5% goat serum. Reactions were developed by incubation with DyLight 488-conjugated donkey anti-guinea pig IgG or Cy3-conjugated goat anti-rabbit IgG (Jackson ImmunoResearch Laboratories; 1:800 dilution).

cDNA Constructs—Constructs used in cell culture experiments were cloned into the pCS2 expression vector. Murine FLAG-EMILIN-1 and FLAG-EMILIN-1ΔEMI cDNAs were described previously (10). Full-length EMILIN-3L and EMILIN-3S cDNAs were obtained from mouse embryo RNA by PCR amplification with the following primers: 5′-AAA GAA TTC CGA GGG ACA GAG TGA CGA C-3′ (forward) and 5′-TTT TCT AGA GTT GGT GGG ATC TGC ACT TT-3′ (reverse). The amplified products were inserted as EcoRI-XbaI fragments in pCS2 vector. For the generation of a FLAG-EMILIN-3 construct, a fragment corresponding to amino acids 32–758 of EMILIN-3 was amplified from full-length EMILIN-3L cDNA by PCR using a forward primer (5′-AAA CTC GAG CAG CCC AGT GCC TCC CGT TAC AG-3′) with an XhoI site at the 5′-end of the cDNA and the same reverse primers as above. The amplified product was cloned into a pCS2 expression construct containing sequences coding for the mouse chordin signal peptide followed by a FLAG epitope tag (Chordin-FLAG-pCS2) (21). The EMILIN-3ΔEMI construct, containing a deletion of amino acid residues 54–189, was generated as follows. A fragment coding for amino acids 1–54 was amplified from full-length EMILIN-3L and FLAG-EMILIN-3 constructs by PCR using SP6 primer (5′-TAC GAT TTA GGT GAC ACT ATA G-3′) and a reverse primer carrying an NdeI restriction site (5′-TTT CAT ATG CTG GCC CCG GGC GCA GC-3′), and the amplified products were cloned as EcoRI-NdeI fragments in the EMILIN-3L or FLAG-EMILIN-3L plasmid, respectively, generating the deleted constructs. The FLAG-EMILIN-1ΔgC1q construct, containing sequences coding for amino acid residues 32–860 of murine EMILIN-1, was obtained from FLAG-EMILIN-1 by PCR amplification with SP6 primer and a specific reverse primer (5′-TTT TCC CTG CTC CCC TTG AGG AC-3′), and the amplified product was cloned into the Chordin-FLAG-pCS2 vector as an XhoI-XbaI fragment. The HA-EMILIN-3 and HA-EMILIN-3ΔEMI were obtained by subcloning the respective XhoI-XbaI fragments into a Chordin-HA-pCS2 vector containing the HA epitope tag. The EMI3-FLAG construct, containing amino acids 1–190 of EMILIN-3L, was obtained by PCR amplification of the full-length EMILIN-3 using the SP6 primer and a reverse primer (5′-CTA CTT ATC GTC GTC ATC CTT GTA ATC ATA TGC TTG CGA CAG GCG CT-3′) carrying the FLAG coding sequence before the stop codon. Mouse constitutively active pro-TGF-β2 (C226S/C228S/C229S) and pro-TGF-β3 (C228S/C230S) were generated by site-directed mutagenesis by overlap extension of cysteine residues essential for latency and located in conserved positions of latency-associated peptide. Two sets of primers, containing the mutation site together with upstream or downstream sequences, respectively, were used in two separate reactions to amplify overlapping DNA fragments. Cysteines 226, 228, and 229 of mouse pro-TGF-β2 were mutated to serines using full-length mouse pro-TGF-β2 cloned in pCMV-SPORT6 plasmid (RZPD) as a template. A fragment spanning from the Eco47III site to the BamHI site of pro-TGF-β2 cDNA was mutated using the following two sets of oligonucleotide primers: 5′-CCA AAG ACT TAA CAT CTC CCA CC-3′ (forward) and 5′-CGA AGG TAC **T**GC **T**GG GGC **T**GT-3′ (reverse with mutations in bold letters) and 5′-AC**A** GCC CC**A** GC**A** GTA CCT TCG-3′ (forward with mutations in bold letters) and 5′-ATG CCC CAG CAC AGA AGT TAG C-3′ (reverse). The mutated DNA was cloned in pGEM-T Easy vector (Promega), sequenced, and subcloned into full-length pro-TGF-β2 by BamHI and Eco47III digestion. The mutated TGF-β2 cDNA was finally subcloned into pCS2 to produce pro-TGF-β2 (C226S/C228S/C229S). Cysteines 228 and 230 of TGF-β3 were mutated using full-length mouse pro-TGF-β3 cloned in pCMV-SPORT6 plasmid as a template. To produce a mutated fragment of pro-TGF-β3 comprising the region between the two BglII sites of the cDNA sequence, three fragments were generated by PCR using the following sets of primers: 5′-CGT TGG ACT TCG GCC ACA TC-3′ (forward) and 5′-CCT ATG TAG CGC TGC TTG GC-3′ (reverse), 5′-CAG CTC CAA GCG CAC AGA AC-3′ (forward) and 5′-GTG TGA C**T**T GGA C**T**G TGG ATG-3′ (reverse with mutations in bold face letters), 5′-CAT CCA C**A**G TCC A**A**G TCA CAC-3′ (forward with mutations in bold letters) and 5′-CCA CCT CTG CCT GCA CCA C-3′ (reverse), and 5′-GAG GCC TGG AGC CCA GAA G-3′ (forward) and 5′-CCA GGG GAC TTT GGC TTG GT-3′ (reverse). Fragments were inserted into pGEM-T easy vector (Promega), sequenced, and subcloned in BglII-restricted full-length pro-TGF-β3. The mutated pro-TGF-β3 cDNA was finally subcloned into pCS2 to produce pro-TGF-β3 (C228S/C230S). Full-length cDNA for human pro-TGFβ1 was a gift from Jorma Keski-Oja (University of Helsinki, Helsinki, Finland). The porcine constitutively active pro-TGF-β1 (C223S/C225S) expression plasmid was obtained from Jeffrey M. Davidson (Vanderbilt University, Nashville, TN). All plasmids were sequenced prior to use.

Cell Transfection, Protein Extracts, and Luciferase Assay—HEK293T cells were cultured in Dulbecco's modified Eagle's medium containing 4.5 g/liter glucose, 25 mM HEPES, 2 mM L-glutamine, and 10% fetal bovine serum (Invitrogen) and maintained at 37 °C in a humidified 5% CO_2 atmosphere. Subconfluent HEK293T cultures were transfected overnight with the indicated plasmids using the calcium phosphate procedure

(22). Cells were washed with phosphate-buffered saline and fed with serum-free medium, and cell lysate and conditioned medium were collected after 48 h. The conditioned media were supplemented with a protease inhibitors mixture (Roche Applied Science). The cell extracts were prepared by lysis in an ice-cold buffer containing 25 mM Tris, pH 7.5, 150 mM NaCl, 2.5 mM EDTA, 10% glycerol, 1% Nonidet P-40, and protease inhibitors. For the preparation of ECM extracts, cells were lysed in culture dishes at 4 °C with RIPA buffer (50 mM NaCl, 25 mM Tris-HCI, pH 7.5, 0.5% Nonidet P-40, 0.5% sodium deoxycholate, 0.1% SDS) supplemented with protease inhibitors. The dishes were then rinsed three times with cold RIPA buffer, and the extracellular material attached to the dish was extracted by scraping at 90 °C in 2× Laemmli sample buffer. Where indicated, cells were treated with 50 μg/ml soluble heparin (Sigma). Glycosylation was assessed by treatment of samples using an Enzymatic Protein Deglycosylation kit (Sigma) following manufacturer's instructions. For luciferase assays, 6×10^4 cells were plated in each well of 24-well plates. The CAGA12-lux reporter (a gift from Peter ten Djike) and the pCMV-LacZ plasmids were used together with the indicated constructs. Cell layers were harvested with luciferase lysis buffer (25 mM Tris-HCl, pH 7.8, 2.5 mM EDTA, 10% glycerol, 1% Nonidet P-40, 2 mM DTT). Luciferase and β-galactosidase activities were measured in each sample, and values of luciferase activity were normalized to β-galactosidase activity to account for differences in transfection efficiencies. Every sample was transfected in triplicate, and every experiment was repeated at least two times.

Immunoprecipitation—For the immunoprecipitation of endogenous EMILIN-3, adult mouse tissues or whole embryos were snap frozen in liquid nitrogen, pulverized by pestle and mortar, and lysed for 30 min at 4 °C in a solution containing 50 mM Tris-HCl, pH 7.5, 150 mM NaCl, 2 mM EDTA, 1% Triton X-100, and protease inhibitors. Tissue extracts were then centrifuged for 90 min at 4 °C, and the supernatants were recovered. Samples were first precleared by incubation for 5 h at 4 °C with 50 μl of protein A-Sepharose (Amersham Biosciences), 2% bovine serum albumin, and 10 μl of preimmune serum. The samples were centrifuged for 2 min at 500 × *g*, and the supernatants were incubated overnight at 4 °C with 10 μl of rabbit EMILIN-3 antiserum and 50 μl of protein A-Sepharose. After centrifugation at 500 × *g*, the precipitates were washed three times with PBS containing 1.5 mM $MgCl_2$ and 0.05% CHAPS (Roche Applied Science), eluted in 2× Laemmli sample buffer, boiled for 3 min, and analyzed by gel electrophoresis. For co-immunoprecipitation of transfected FLAG-EMILIN-3 and HA-EMILIN-3, transfected HEK293T cells were harvested in cold RIPA buffer, and cell lysates were immunoprecipitated by overnight incubation at 4 °C with an anti-FLAG resin (Sigma). After three washes in cold RIPA buffer, precipitated material was eluted in 2× Laemmli sample buffer, boiled for 3 min, separated by gel electrophoresis, and analyzed by Western blot with an anti-HA antibody (Sigma; 1:1000 dilution).

Gel Electrophoresis and Western Blot—Unreduced samples were subjected to SDS-PAGE on 3–8% (w/v) gradient polyacrylamide gels or composite 2.4% acrylamide, 0.5% agarose gels. Where indicated, samples were reduced by addition of 200 mM DTT and subjected to SDS-PAGE on 4–12% (w/v) gradient polyacrylamide gels. For Western blot, proteins were electrophoretically transferred to nitrocellulose membranes. The membrane was saturated with 5% nonfat milk in Tris-buffered saline with 0.1% Tween 20 and incubated in the same buffer with rabbit and guinea pig affinity-purified anti-EMILIN-3 (1:1000–1:3000 dilution), rabbit polyclonal anti-FLAG (Sigma; 1:3000 dilution), or mouse monoclonal anti-HA (Sigma; 1:1000 dilution) antibody. Membranes were incubated with the appropriate horseradish peroxidase-conjugated secondary antibody (Amersham Biosciences), and reacting bands were revealed by chemiluminescence with SuperSignal West Pico or SuperSignal West Dura (Pierce). For gel electrophoresis after partial reduction, protein samples were reduced with DTT at final concentrations of 0–10 mM at 37 °C for 45 min. Subsequent alkylation of the samples was done by adding iodoacetamide to a final concentration of 25 mM and incubation for 30 min at room temperature in the dark. The samples were then subjected to SDS-PAGE on a 4–10% (w/v) gradient polyacrylamide gel, and proteins were visualized by staining with Coomassie Brilliant Blue G-250.

Circular Dichroism Spectroscopy—Circular dichroism spectra were recorded in a Jasco J-715 spectropolarimeter using a thermostated 1-mm-path length quartz cell (Hellma). Proteins were dissolved in 10 mM Tris, 150 mM NaCl, pH 7.4 at a concentration of 0.3 mg/ml. Samples were reduced by adding DTT to a final concentration of 10 mM and incubating the sample for 45 min at 37 °C. The far-ultraviolet spectra (195–250 nm) were measured at 20 °C. After subtraction of the buffer contribution, data were converted to mean molar residue ellipticity. Secondary structures were calculated with the online server DICHROWEB (23) using the K2D algorithm (24). Melting curves were recorded at a fixed wavelength of 220 nm while the sample was heated up to 90 °C at a rate of 12 °C/h. The reversibility of the unfolding was tested by gradual cooling to 20 °C.

RESULTS

Structure and Domain Organization of Mouse EMILIN-3—The murine *Emilin3* gene (Mouse Genome Informatics Database MGI:2389142) spans about 6.4 kb and contains four exons separated by three relatively small introns. Mouse *Emilin3* cDNA (GenBank™ accession number NM_182840) contains an open reading frame of 2277 bp and encodes for a protein of 758 amino acids including a signal peptide of 21 residues (Fig. 1, *A* and *B*). The mature secreted protein has a calculated molecular mass of 82.5 kDa. At its N-terminal end, EMILIN-3 contains an EMI domain of 79 amino acid residues with an identity of 52.6 and 53.9% when compared with the EMI domain of EMILIN-1 and EMILIN-2, respectively, whereas the overall identity with these two proteins is about 20%. Database comparisons did not identify any other known domain within EMILIN-3. mRNA analysis (see also below) revealed that murine EMILIN-3 has two splicing isoforms, hereafter referred to as EMILIN-3L and -3S with the shorter one lacking the first 141 bp of the fourth exon (Fig. 1*B*).

Sequence analysis with the COILS program (25) predicted several regions with a high probability of forming coiled coil structures at the C-terminal end of the protein (Fig. 1*C*). Coiled coil regions contain only α-helices as secondary structure ele-

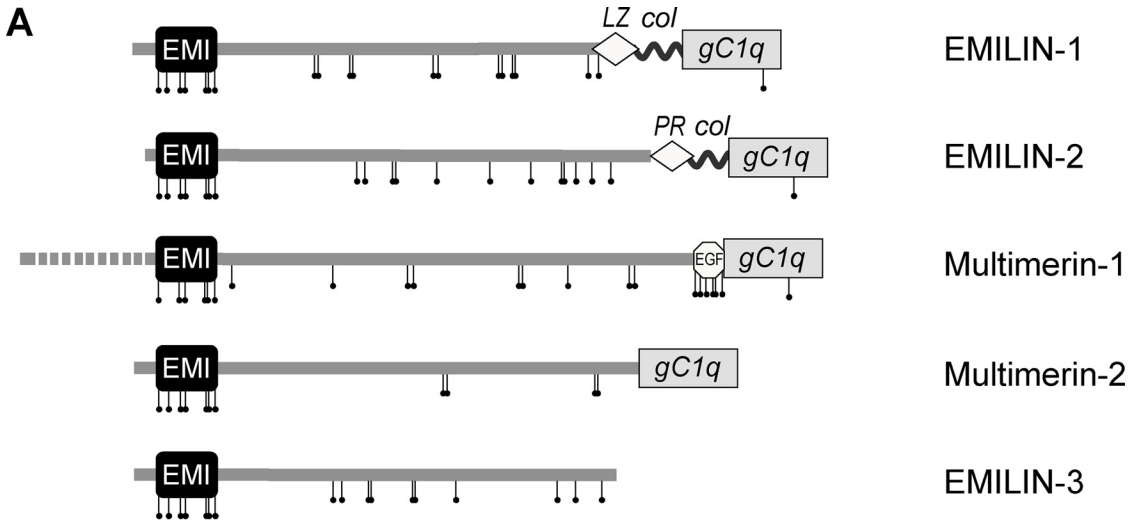

B

```
                    20                  40                  60
MGRRLSVWLC TVAALLSGAQ AKGTPLLARP AQPSASRYSL YTTGWRPRLR PGPHKSLCAY
                    80                  100                 120
VVHRNVTCVL QEGAESYIKA EYRNCGWGPN CPSTVRYRTV FRPRYKIGYK TVTDLAWRCC
                   140                 160                 180
PGLTGESCPE HLTDHGATPP HQEPEPQIPL GQLGPGPRPS PYSREAPRPR GRKGQGPFGE
                   200                 220                 240
RLEQRLSQAY GTLSGLVASH ENPNRITGDS RAPVVPIGFG VIPEGLVAPE DRGRGPLIPP
                   260                 280                 300
LSEILSKVTE VSNTLQTKVQ LLDEVRGLAL GHEAHLQRLR EAPPSPLTSL ALLEEYVDQR
                   320                 340                 360
LQRLWGSLLD GFEQKLQGVQ SECDLRVQEV RQQCEEGQAA SQRLHQSLDG RELALRRELS
                   380                 400                 420
QLGTQLQGLT LTGGGTCCSQ LALISARVDS LERNLQAVTE TQGGPGTLAA DELARLSAAM
                   440                 460                 480
LQGGVDGLLE GLETINGTEN GARGCCLRME VGGWGVGGFG STLEQRVQSL EERLATLTGE
                   500                 520                 540
LSPESAIPDR SARPLVHSEL AVLEQRLVSL ETSCTPSTTT AILDNLVAEV KAWQSRSEAL
                   560                 580                 600
LHQVARHTAL LQQLNGTVAE VQGQLAEGTG SSLQGEITLL KVNLNSVSKS LTGLSDSVSQ
                   620                 640                 660
YSDAFSAANT SLDERERRVE AEVHTIQEQI SSQGSRLQAG HRQVLNLRGE LEQLKAGMAN
                   680                 700                 720
VARGLSRCRD TAQELQHTVG HFDQRVAQVE GACERLGLLA THLNSLPTEQ LRSREGLWGH
                   740
IDKLNHTLAQ HTQDIARLRD DLLDCRAQLA EVRPGRAD
```

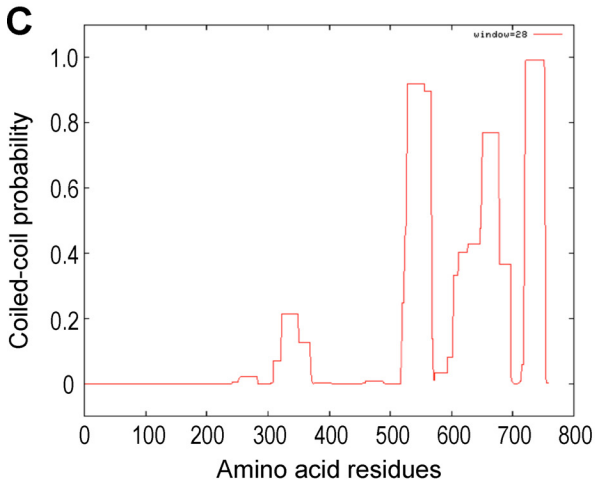

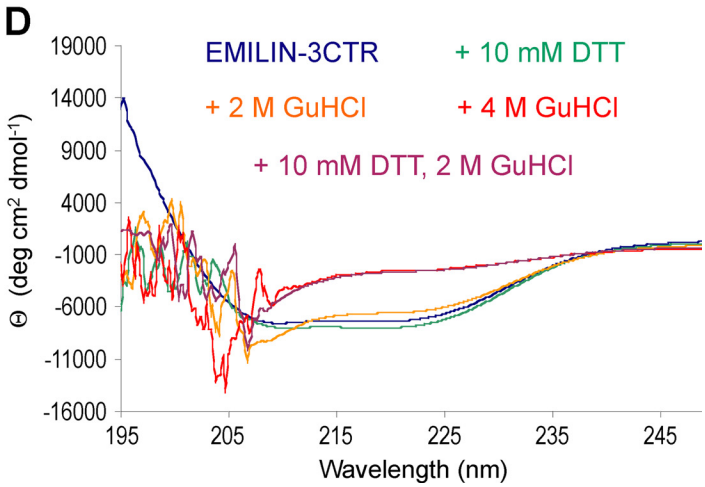

TABLE 1
Secondary structure content of EMILIN-3CTR
Values were calculated using the DICHROWEB program (23).

	NRMSD[a]	α-Helix	β-Sheet	Random coil
EMILIN-3CTR	0.072	0.31	0.14	0.56
EMILIN-3CTR + 10 mM DTT	0.107	0.26	0.14	0.60
EMILIN-3CTR + 2 M GdnHCl	0.106	0.31	0.12	0.58

[a] Normalized root mean square deviation.

ments, and the α-helix conformation can be stabilized by oxidized cysteine residues (26, 27). To verify coiled coil formation, a recombinant fragment of EMILIN-3 corresponding to the C-terminal region of the protein (EMILIN-3CTR; amino acid residues 171–758) was generated and analyzed by circular dichroism spectroscopy to determine the α-helix content (Fig. 1*D*). The far-ultraviolet spectrum of the oxidized EMILIN-3CTR showed slight minima at 208 and 222 nm, indicating that parts of the protein have an α-helical conformation. The secondary structure analysis algorithm K2D gave a good fit with a normalized root mean square deviation of 0.072 and yielded an α-helical content of about 31% (Table 1). This value is in agreement with the fact that only the C-terminal third of EMILIN-3CTR is predicted to form coiled coil structures (Fig. 1*C*). The N-terminal part of EMILIN-3CTR is likely to form random coils and other secondary structures as circular dichroism spectroscopy indicated that EMILIN-3CTR contains about 50% random coil. After reduction of EMILIN-3CTR with 10 mM DTT, the α-helical content decreased slightly to about 26%, suggesting that disulfide bonds stabilize the coiled coil region. This could also be shown after addition of the denaturing agent guanidine hydrochloride (GdnHCl). All ordered structures of oxidized EMILIN-3CTR were lost when the protein was treated with 4 M GdnHCl. In the presence of 2 M GdnHCl, 30% α-helix was detected, whereas reduced EMILIN-3CTR lost all secondary structure after the addition of 2 M GdnHCl (Fig. 1*D*). Both GdnHCl and DTT disturbed the spectra at wavelengths below 210 nm, but assessment of α-helical content was still possible.

To monitor the thermal transition from coiled coil α-helix to random coil, oxidized EMILIN-3CTR and reduced EMILIN-3CTR were analyzed by circular dichroism at 220 nm while samples were heated to 90 °C (supplemental Fig. S1A). As only parts of EMILIN-3CTR appear to form coiled coil structures, it was not surprising that the thermal denaturation curves were complex, not allowing the calculation of distinct melting points. However, for both the oxidized EMILIN-3CTR and reduced EMILIN-3CTR, heat denaturation was partially reversible after cooling the sample to 20 °C. After complete denaturation in the presence of 4 M GdnHCl or 2 M GdnHCl and 10 mM DTT, no refolding was observed (supplemental Fig. S1B).

Expression of EMILIN-3 during Mouse Embryonic and Postnatal Development—We first investigated EMILIN-3 expression by RT-PCR analysis. EMILIN-3 mRNA was detected in preimplantation mouse blastocysts and in a few human and murine cell lines (Fig. 2*A* and supplemental Fig. S2). During mouse postimplantation development, EMILIN-3 transcripts were present at all studied stages with stronger expression during midgestation (Fig. 2*B*). RT-PCR analysis of various tissues derived from neonatal and adult mice showed that, similar to other EMILIN/Multimerin genes, EMILIN-3 expression decreases after birth. In adult mice, EMILIN-3 transcripts were found only in a few of the examined tissues, namely testis, eye, and brain (Fig. 2*C*). When using oligonucleotide primers for the two EMILIN-3 isoforms, both fragments corresponding to EMILIN-3L and -3S were detected in mouse embryos and postnatal tissues, confirming that these are *bona fide* mRNA splicing isoforms (Fig. 2, *B* and *C*). Northern blot analysis of newborn mouse tissues showed that EMILIN-3 mRNA migrates at about 3.8 kb and confirmed expression in postnatal testis, uterus, and intestine (Fig. 2*D*).

We further analyzed EMILIN-3 mRNA expression by *in situ* hybridization of whole-mount E8.5 and E9.5 embryos and serial sections derived from E10.5–E14.5 embryos. At E8.5, EMILIN-3 mRNA was detected at low levels in the tail bud, whereas at E9.5, expression became more abundant in the tail bud region with also a faint labeling in the primitive hindgut (supplemental Fig. S3). At E10.5, strong expression was detected in the esophageal bud, the mesenchyme of branchial arches, the tail bud, and a small region of the developing midbrain (data not shown). Expression in the midbrain, now confined to the ventricular zone of the third ventricle, was still present at both E11.5 and E12.5 and disappeared at E13.5 (Fig. 3, *A–C*, and data not shown). During organogenesis, EMILIN-3 was strongly expressed throughout the gastrointestinal tract. At earlier stages (E10.5–E12.5), EMILIN-3 mRNA was diffusely present in the wall of the gastrointestinal system from the esophagus to the hindgut (Fig. 3, *A* and *D*). Starting from E13.5, EMILIN-3 transcripts became restricted to a thin layer corresponding to the myenteric plexus, showing a craniocaudal gradient with strongest signal in the esophagus (Fig. 3, *E–H*). At E13.5, expression became abundant in the subepidermal mes-

FIGURE 1. **Amino acid sequence of murine EMILIN-3 and evidence for coiled coil α-helical region.** *A*, schematic diagram of the structure of mouse EMILIN/Multimerin proteins. *Col*, short collagenous region; *EGF*, EGF-like domain; *EMI*, EMI domain; *gC1q*, globular C1q domain; *LZ*, leucine zipper motif; *PR*, proline-rich region. Cysteine residues are marked by *vertical bars*. The *dashed line* in Multimerin-1 indicates a cleaved propeptide region. *B*, murine EMILIN-3 amino acid sequence as derived from the full-length cDNA. An *arrow* marks the putative signal peptide cleavage site. The EMI domain is *underlined*, and the seven conserved cysteine residues are marked by *asterisks*. *Arrowheads* indicate four sites predicted to be *N*-glycosylated. The *dotted underline* indicates the sequence that can be removed by alternative splicing. *C*, prediction of coiled coil formation as deduced by analysis with the COILS program. Three regions with high probability of forming coiled coil structures are predicted in the C-terminal part of murine EMILIN-3 sequence. *D*, circular dichroism spectra revealing the presence of about 31% α-helix in the EMILIN-3CTR recombinant fragment (amino acid residues 171–758). The α-helical structure was lost upon treatment with 4 M GdnHCl (*GuHCl*) or 2 M GdnHCl together with 10 mM DTT. *θ*, mean molar residual ellipticity; *deg*, degrees.

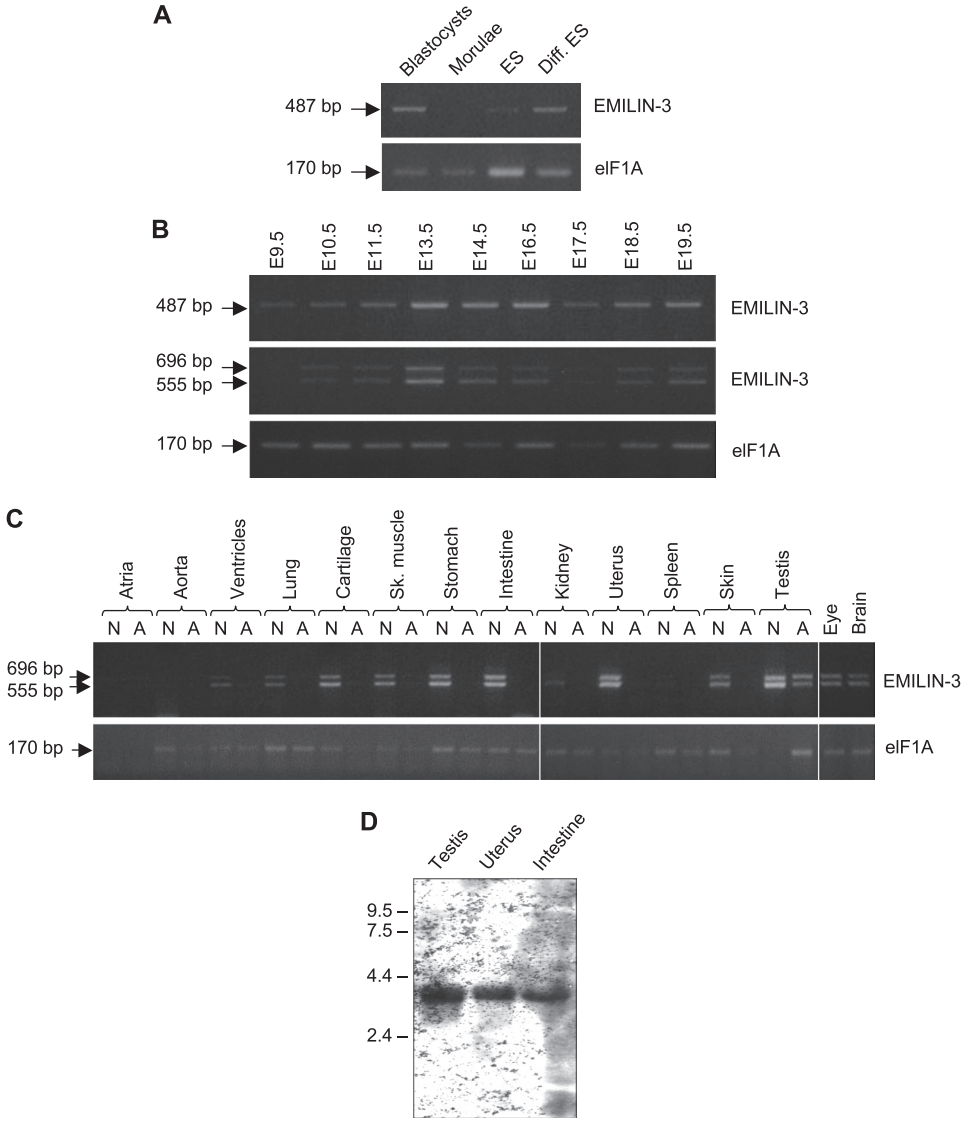

FIGURE 2. **Detection of EMILIN-3 mRNA transcripts during mouse development and in postnatal and adult mouse tissues.** *A–C*, RT-PCR analysis of total RNA derived from whole mouse embryos at the indicated developmental stages (*A* and *B*) or from postnatal and adult mouse tissues (*C*). Semiquantitative RT-PCR was carried out using oligonucleotide primers able to detect either all EMILIN-3 transcripts or the two splicing variants differing by 141 base pairs. Amplification of eIF1A was used as an RNA loading control. *D*, Northern blotting identification of EMILIN-3 mRNA in newborn mouse tissues. The migration of molecular weight markers is indicated in kb on the *left*. *A*, adult; *Diff. ES*, differentiated mouse embryonic stem cells; *ES*, undifferentiated mouse embryonic stem cells; *N*, neonatal; *Sk.*, skeletal.

enchyme (Fig. 3*I*). Genital ridges were strongly labeled throughout their development, whereas metanephric tissues and kidney were negative (Fig. 3, *J–L*). Expression of EMILIN-3 was also found in the intervertebral discs, the region surrounding the main branches of alveoli, the mesenchymal tissue around vibrissae, the diaphragm, and the cephalic mesenchyme (Fig. 3, *M–Q*). A strong expression was also detected in the perichondrium around sites of bone and cartilage formation in trunk, skull, and limbs (Fig. 3, *R* and *S*). In contrast to other EMILIN/Multimerin genes, EMILIN-3 expression was not detected in the cardiovascular system at any developmental stage (Fig. 3, *A* and *M*, and supplemental Fig. S3).

EMILIN-3 Has Restricted Distribution in Adult Mouse Tissues—As specific antibodies for EMILIN-3 were not available, guinea pigs and rabbits were immunized with recombinant EMILIN-3CTR. After affinity purification, both guinea pig and rabbit antibodies detected EMILIN-3, and their specificity was confirmed by Western blot and immunofluorescence (supplemental Figs. S4–S6).

To investigate EMILIN-3 protein distribution, we carried out immunofluorescence on frozen sections from adult mouse tissues. EMILIN-3 antisera raised in guinea pig and rabbit gave very similar results, and immunofluorescence data obtained with the guinea pig antibody are shown here. EMILIN-3 displayed a restricted protein distribution in adult tissues (Fig. 4). In agreement with the mRNA expression, a conspicuous labeling was detected in testis where EMILIN-3 was abundantly deposited in the collagenous structure of the tunica albuginea and the basement membrane surrounding each seminiferous tubule (Fig. 4, *A–C*). Conversely, EMILIN-3 distribution in ovary was confined to the tunica albuginea, and no labeling was found in cortical and medullary regions or around follicles (Fig.

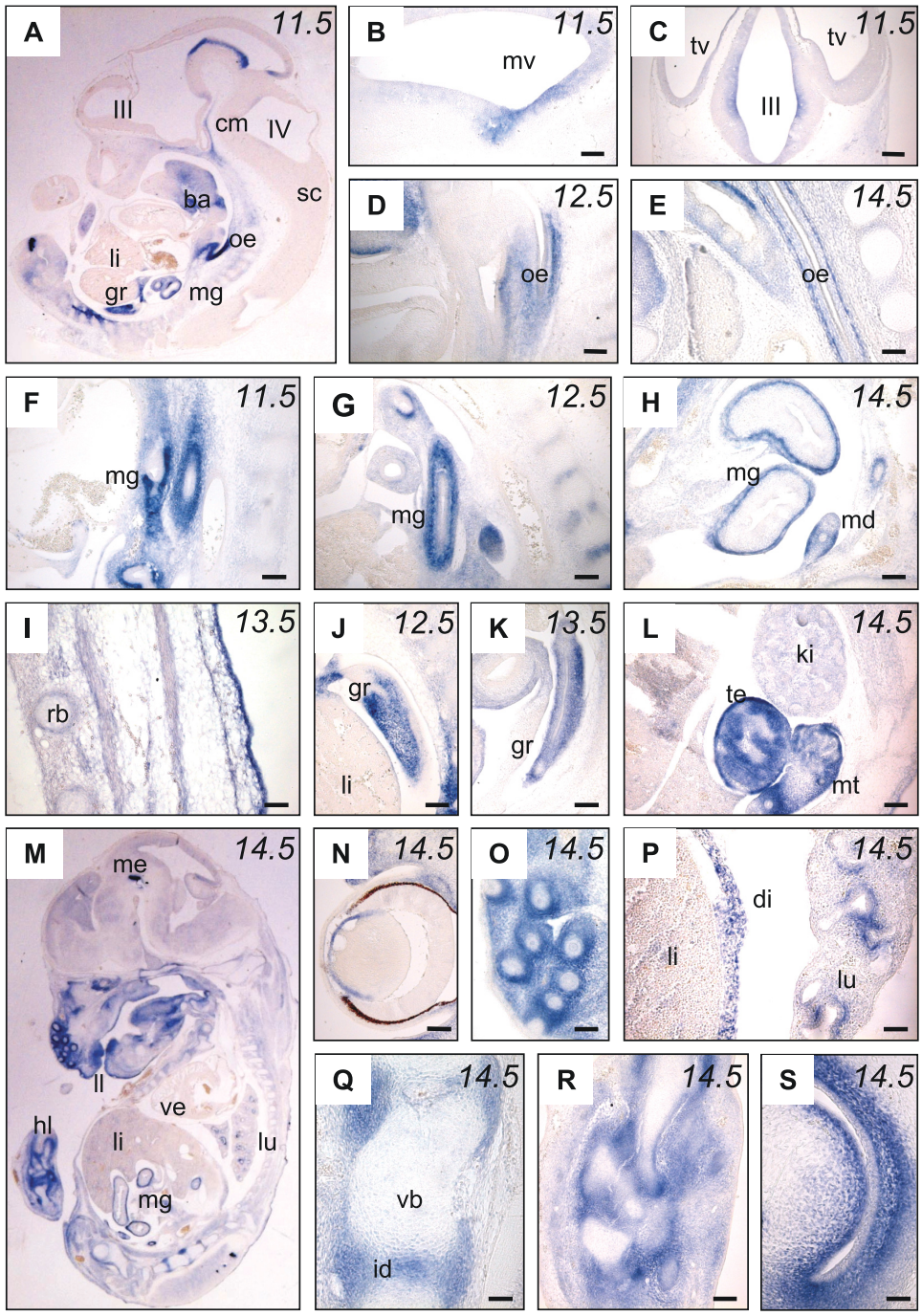

FIGURE 3. ***In situ*** **hybridization analysis of EMILIN-3 mRNA expression during mouse embryonic development.** Mouse embryos at different developmental stages (E11.5–E14.5) were processed and analyzed by *in situ* hybridization on paraffin sections with an EMILIN-3 antisense probe. *A*, parasagittal section of whole E11.5 embryo. *B* and *C*, sagittal and transverse sections, respectively, at E11.5 showing EMILIN-3 expression in the ventricular zone of ventral midbrain. *D–H*, expression in the gastrointestinal tract was detected at all stages starting from E11.5; esophagus (*D* and *E*) and midgut (*F–H*) are shown. *I–L*, expression in the subepidermal mesenchyme of trunk (*I*), genital ridges (*J* and *K*), and mesonephric tissue (*L*). *M*, parasagittal section of whole E14.5 embryo. *N–S*, details of E14.5 sections showing EMILIN-3 expression in the developing eye (*N*), vibrissae (*O*), diaphragm and main bronchi (*P*), intervertebral discs (*Q*), perichondrium of the hind limbs (*R*), and inner ear (*S*). *III*, third ventricle; *IV*, fourth ventricle; *ba*, branchial arches; *cm*, cephalic mesenchyme; *di*, diaphragm; *gr*, genital ridge; *hl*, hind limb; *id*, intervertebral discs; *ki*, kidney; *li*, liver; *ll*, lower lip; *lu*, lung; *md*, mesonephric duct; *me*, mesencephalon; *mg*, midgut; *mt*, mesonephric tissue; *mv*, mesencephalic vesicle; *oe*; esophagus; *rb*, rib primordia; *sc*, spinal cord; *te*, testis; *tv*, telencephalic vesicle; *vb*, vertebral bodies; *ve*, ventricle. *Scale bar*, 50 (*I*, *P*, and *Q*) or 100 μm (other panels).

4*D*). A diffuse staining was detected in the wall of the uterus (Fig. 4*E*). Strong labeling for EMILIN-3 was found in the external ear where the protein localizes in the perichondrium of the elastic cartilage (Fig. 4*F*). EMILIN-3 was also detected in skeletal muscles, but the distribution was variable among different muscles. For example, in quadriceps, the endomysium of many (but not all) myofibers was labeled, and in tibialis anterior, staining was restricted to the epimysium, whereas the diaphragm was negative (Fig. 4, *G* and *H*, and data not shown). EMILIN-3 showed a peculiar distribution throughout the gas-

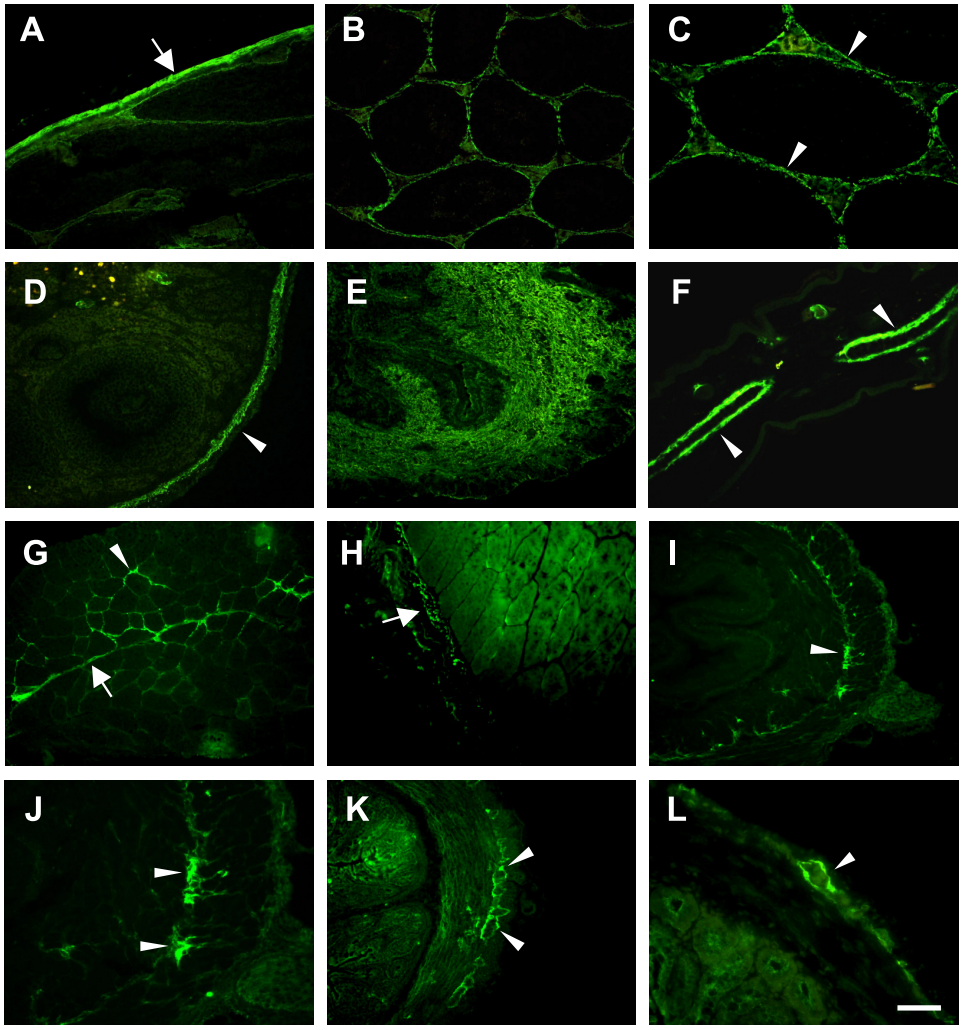

FIGURE 4. **EMILIN-3 has restricted protein distribution in adult tissues.** Adult mouse tissues were processed and analyzed by immunofluorescence with the affinity-purified guinea pig EMILIN-3 antibody. *A–C*, sections from adult testis with abundant EMILIN-3 deposition in the tunica albuginea (*arrow*) and at the level of basement membranes of seminiferous tubules (*arrowheads*). *D*, in ovary, staining is detectable only in the tunica albuginea (*arrowhead*). *E*, section of uterus wall showing a diffuse labeling for EMILIN-3. *F*, transverse section of the external ear showing strong EMILIN-3 deposition in the perichondrium surrounding elastic cartilage (*arrowheads*). *G*, section of quadriceps muscle where labeling is found in the perimysium (*arrow*) and endomysium (*arrowheads*) of several myofibers. *H*, section of tibialis anterior muscle showing staining of the epimysium (*arrow*). *I–L*, transverse sections of esophagus (*I* and *J*) and colon (*K* and *L*) revealing strong labeling at the level of the myenteric plexus (*arrowheads*). *Scale bar*, 50 (*C*, *H*, *J*, and *L*) or 100 μm (other panels).

trointestinal tract from esophagus to colon where immunofluorescence was found in a thin region between the longitudinal and transverse smooth muscle layers corresponding to the myenteric plexus (Fig. 4, *I–L*). In contrast to other EMILINs/Multimerins, EMILIN-3 was totally absent in the cardiovascular system, and parenchymatous organs, such as heart, blood vessels, kidneys, spleen, and liver, were completely negative for EMILIN-3 immunostaining (supplemental Fig. S7 and data not shown).

EMILIN-3 Forms Disulfide-bonded Homotrimers and High Molecular Weight Multimers and Carries N-Glycans—Immunoprecipitation and Western blotting of adult mouse tissue extracts with the two EMILIN-3 antisera showed a major band migrating at about 105 kDa, which is consistent with the expected molecular mass of the protein (Fig. 5*A*). Interestingly, even under strong reducing conditions, a fraction of the protein migrated as discrete bands with lower mobility; their calculated molecular masses (210 and 315 kDa) are in agreement with the potential formation of dimers and trimers. Some protein was also detected at the gel origin, suggesting a strong tendency of EMILIN-3 to form high molecular weight aggregates. Western blot analysis under reducing conditions of immunoprecipitated EMILIN-3 extracts from whole E14.5 embryos resulted in a doublet of bands at about 95 and 105 kDa (Fig. 5*B*), which may correspond to the two splicing isoforms detected by RT-PCR experiments. When analyzed by SDS-PAGE under non-reducing conditions, immunoprecipitated EMILIN-3 material migrated in two distinct regions of the gel with a lower band at about 105 kDa, corresponding to the size of the monomeric protein, and a broad band migrating between the 268 and 460 kDa size markers, suggesting that *in vivo* EMILIN-3 largely exists as cysteine-bound oligomers (Fig. 5*B*).

To further explore the biochemical properties of EMILIN-3, we carried out transient transfection experiments of HEK293T cells with full-length expression constructs coding for EMILIN-3L and EMILIN-3S. Cell lysates and conditioned media were collected and analyzed by Western blotting. Under

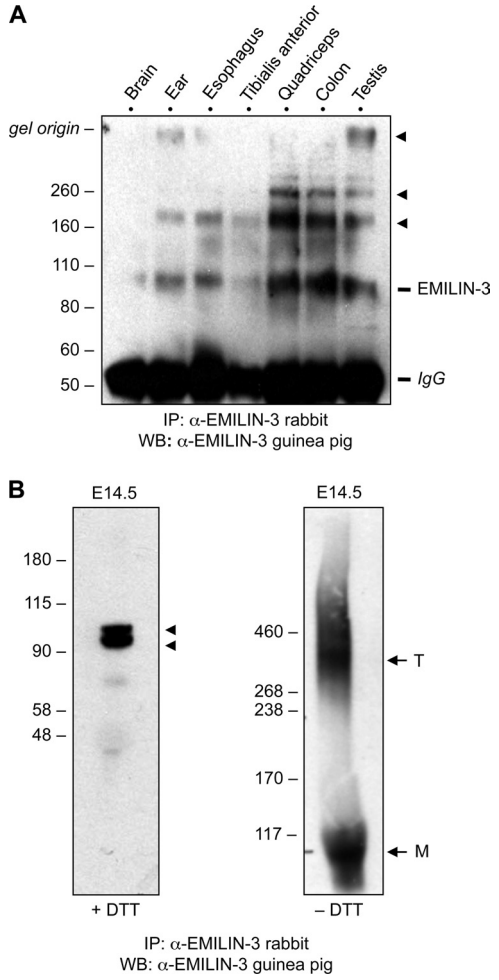

FIGURE 5. **Immunoprecipitation of EMILIN-3 from adult mouse tissues and whole embryo extracts.** *A*, immunoprecipitation of protein extracts from different adult tissues with affinity-purified rabbit EMILIN-3 antiserum followed by SDS-PAGE on a 4–12% gradient gel under reducing conditions and Western blot with affinity-purified guinea pig EMILIN-3 antibodies. A major band migrating at about 105 kDa and corresponding to the EMILIN-3 monomeric form is present in most tissues together with a ladder of slower migrating bands above 200 kDa (*arrowheads*) probably representing partially unreduced EMILIN-3 dimers and multimers. The abundant band migrating at about 55 kDa corresponds to IgG. *B*, immunoprecipitation from whole E14.5 embryo extracts followed by SDS-PAGE on a 4–12% gradient gel under reducing conditions (+ *DTT*; *left panel*) or on a 3–8% gradient gel under non-reducing conditions (− *DTT*; *right panel*) and Western blot for EMILIN-3. Two distinct EMILIN-3 bands migrating at about 95 and 105 kDa (*arrowheads*) are present in reduced E14.5 extracts. Under non-reducing conditions, EMILIN-3 migrates as a broad band at about 100 kDa and a larger diffuse product at about 300 kDa, a molecular mass compatible with homotrimer formation. Migration of protein size markers is indicated in kDa on the *left* of each panel. *IP*, immunoprecipitation; *M*, monomers; *T*, trimers; *WB*, Western blot.

reducing conditions, EMILIN-3L and EMILIN-3S migrated at about 105 and 95 kDa, respectively. Conversely, under non-reducing conditions, the two transfected proteins migrated at about 300 and 270 kDa (Fig. 6*A*), which is consistent with the formation of trimers as observed *in vivo* for the endogenous EMILIN-3. To investigate the nature of these higher molecular weight products and assess whether EMILIN-3 may form homo-oligomers, we generated FLAG- and HA-tagged constructs of full-length EMILIN-3 or EMILIN-3 lacking the EMI domain (EMILIN-3ΔEMI where amino acids 54–189 were missing). After cotransfection of these constructs in HEK293T cells, we immunoprecipitated cell lysates with an anti-FLAG antibody and found that HA-tagged proteins were coprecipitated, strongly suggesting that EMILIN-3 complexes are composed of disulfide-linked homo-oligomers. EMILIN-3ΔEMI coprecipitated with full-length EMILIN-3, indicating that the EMI domain is not required for EMILIN-3 homo-oligomerization (Fig. 6*B*). To further confirm these results, we studied the oligomerization of the EMILIN-3CTR recombinant protein by SDS-PAGE after treatment with increasing concentrations of the reducing agent DTT. In the absence of DTT, the major band migrated at 270–300 kDa in agreement with the calculated mass of trimeric EMILIN-3CTR. With increasing reduction, the trimer band became weaker, and a doublet at about 160 kDa and a band at 80 kDa appeared, indicating that reduction of the trimer in the presence of SDS led to the formation of dimeric and monomeric forms of EMILIN-3CTR. Apparently two dimer forms occur that are presumably connected by different disulfide bonds after partial reduction (Fig. 6*C*).

It has been proposed that the C-terminal gC1q domain of EMILIN-1 plays a role in multimer formation (11). Because EMILIN-3 is able to form disulfide-bonded homotrimers even in the absence of a gC1q domain, we investigated whether the cysteine-rich EMI domain plays any role in the formation of the higher order multimers of EMILIN-3 and EMILIN-1. Toward this aim, FLAG-tagged EMILIN-1 constructs lacking either the EMI domain (EMILIN-1ΔEMI) or the gC1q domain (EMILIN-1Δg1q) were produced and transfected into HEK293T cells in parallel with FLAG-tagged EMILIN-3 and EMILIN-3ΔEMI constructs. Extracts from transfected cells were analyzed by electrophoresis and Western blot under reducing and non-reducing conditions. Under non-reducing conditions, all the recombinant proteins were able to form homotrimers, suggesting that neither the gC1q domain nor the EMI domain is necessary for this process (Fig. 7*A*). Further assembly into higher order multimers was studied by electrophoresis in composite acrylamide-agarose gels under non-reducing conditions. EMILIN-1, EMILIN-1ΔgC1q, and EMILIN-3 were found almost exclusively as large aggregates reaching a size of about 1000–2000 kDa. Conversely, EMILIN-1ΔEMI and EMILIN-3ΔEMI aggregated with a lower efficiency. In particular, almost no high molecular weight aggregates of EMILIN-1ΔEMI could be detected (Fig. 7*B*). Altogether, these data indicate that the gCq1 domain is not strictly required for trimer and multimer formation and suggest a role for the EMI domain in the formation of higher order multimers.

Because the amino acid sequence of EMILIN-3 gives a predicted molecular mass of 82.5 kDa and contains four putative *N*-glycosylation sites, we investigated whether the migration of full-length EMILIN-3 at 105 kDa as detected by SDS-PAGE under reducing conditions was the result of post-translational modifications. Cell lysates and concentrated conditioned media of EMILIN-3-transfected cells were treated with different deglycosylating enzymes and subjected to SDS-PAGE and immunoblotting. This analysis showed that EMILIN-3 undergoes extensive *N*-glycosylation because treatment with endoglycosidase F shifted EMILIN-3 migration to its predicted molecular weight (Fig. 7*C*).

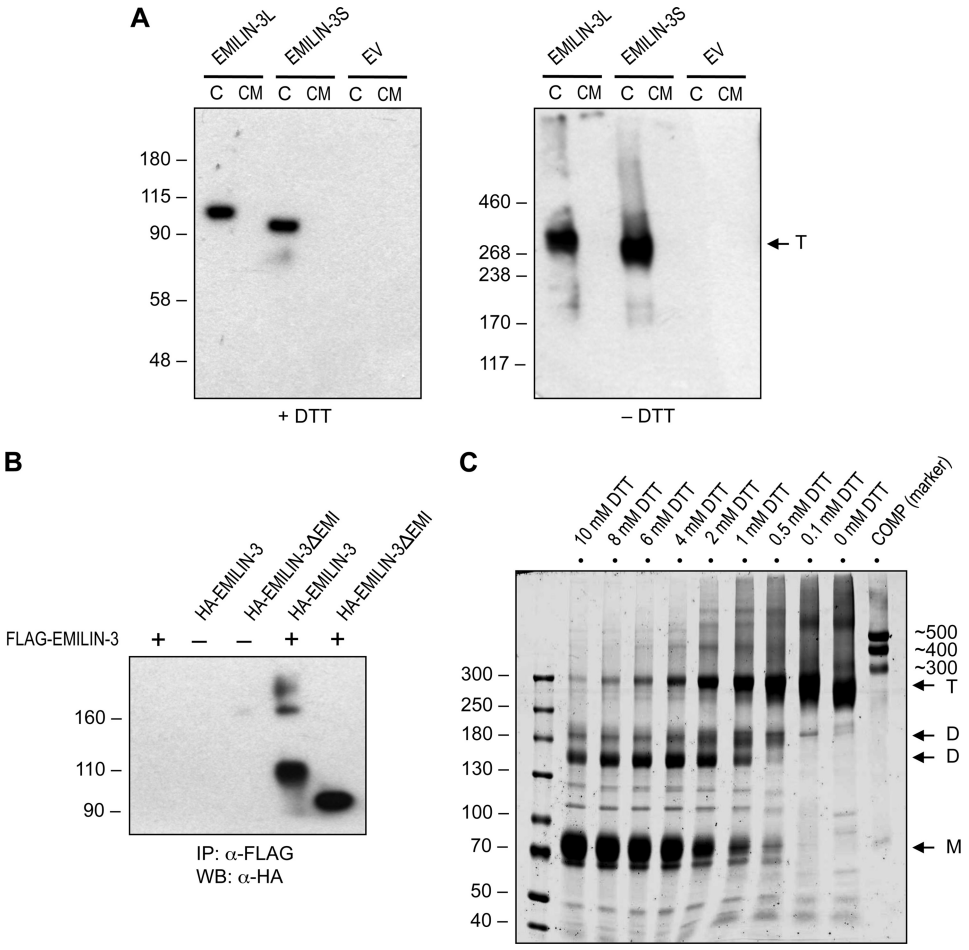

FIGURE 6. **EMILIN-3 forms disulfide-bonded homotrimers.** *A*, HEK293T cells were transfected with the indicated expression constructs. The cell layer and conditioned medium were separated by 4–12% gradient SDS-PAGE under reducing conditions (+ *DTT*; *left panel*) or by 3–8% gradient SDS-PAGE under non-reducing conditions (− *DTT*; *right panel*) and analyzed by Western blot with rabbit EMILIN-3 antiserum. Both transfected EMILIN-3L and -3S proteins were readily detected in the cell extracts but not in the conditioned media. The mobility of transfected EMILIN-3 proteins under non-reducing conditions suggests trimer (*T*) formation. Transfection with the empty vector was used as a control. *B*, HEK293T cells were transfected with HA-tagged EMILIN-3 or HA-tagged EMILIN-3ΔEMI in the presence (+) or in the absence (−) of FLAG-tagged EMILIN-3. Anti-FLAG immunoprecipitation was performed on cell lysates, and samples were separated by 4–12% gradient SDS-PAGE under reducing conditions and analyzed by Western blot with anti-HA antibody. *C*, SDS-PAGE of partially reduced EMILIN-3CTR on a 4–10% polyacrylamide gel. Although oxidized EMILIN-3CTR migrates only as a trimer (*T*) and higher aggregates, reduction releases dimeric (*D*) and monomeric (*M*) protein fragments. Non-reduced cartilage oligomeric matrix protein (COMP) was used as a marker. Migration of protein size markers is indicated in kDa on the *left* of each panel. *C*, cell layer; *CM*, conditioned medium; *EV*, empty vector; *IP*, immunoprecipitation; *WB*, Western blot.

EMILIN-3 Binds Heparin through Its EMI Domain and Is Associated with ECM via Heparin or Heparan Sulfate Proteoglycans—Despite the relatively high levels of transfected EMILIN-3 observed in cell extracts, the protein was barely detectable in conditioned media (see Fig. 6*A*). To further investigate this finding, HEK293T cells were transfected with expression constructs coding for either EMILIN-1, EMILIN-2, or EMILIN-3 protein fused to a FLAG epitope and a heterologous chordin signal peptide, and cell lysates and conditioned media were analyzed by Western blot under reducing conditions with an anti-FLAG antibody. Although EMILIN-1 and EMILIN-2 proteins were detected in both samples, EMILIN-3 could not be detected in the conditioned medium (supplemental Fig. S8A). Therefore, the absence of EMILIN-3 in conditioned media was not dependent on its own signal peptide. Immunofluorescence analysis of cells following cotransfection of EMILIN-3 with a cDNA coding for an endoplasmic reticulum probe revealed that EMILIN-3 colocalized with endoplasmic reticulum, indicating that transfected EMILIN-3 was in the cell secretory pathway. Moreover, some immunolabeling was also found outside the cells, confirming that EMILIN-3 is indeed secreted by transfected cells and that the protein can be found in the extracellular space (supplemental Fig. S8B).

The lack of EMILIN-3 in the conditioned media of transfected cells despite its presence in the secretory pathway and on culture coverslips suggested that the protein might become readily bound to the ECM once secreted. Therefore, we examined the insoluble material that remained associated with the culture dish of HEK293T cells transfected with EMILIN-3 constructs. Protein extracts were prepared by lysing cells in the culture dish with RIPA buffer at 4 °C. After removal of the cell lysate, culture dishes were washed three times with RIPA buffer, and the extracellular material still bound to the dish was extracted with Laemmli buffer at 90 °C. Western blot analysis revealed that the insoluble ECM fraction contained a noticeable amount of EMILIN-3 (Fig. 8*A*). Interestingly, ECM-associated EMILIN-3 migrated slightly more slowly than the protein associated with the cell layer, sug-

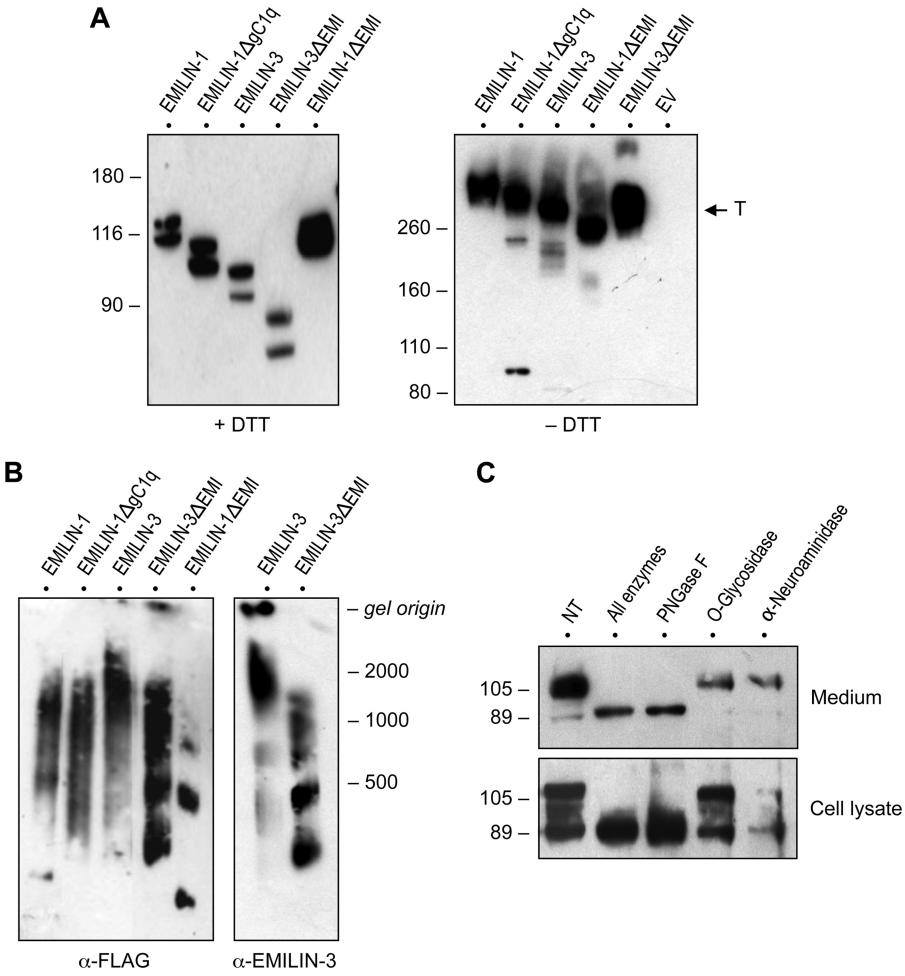

FIGURE 7. **EMILIN-3 undergoes oligomerization and is *N*-glycosylated.** *A*, lysates of HEK293T cells transfected with the indicated plasmids were separated by 4–12% gradient SDS-PAGE under reducing conditions (+ *DTT*; *left panel*) or by 3–8% gradient SDS-PAGE under non-reducing conditions (− *DDT*; *right panel*) followed by Western blot with anti-FLAG antibody. All the tested recombinant proteins migrated at the expected sizes and formed disulfide-linked homotrimers under non-reducing conditions. *B*, lysates of HEK293T cells transfected with the indicated plasmids were separated by electrophoresis on composite 2.4% acrylamide, 0.5% agarose gels under non-reducing conditions and analyzed by Western blot with anti-FLAG or anti-EMILIN-3 antibodies. *C*, HEK293T cells were transfected with the FLAG-tagged EMILIN-3 construct. Cell lysate and acetone-precipitated conditioned medium were treated with the indicated enzymes and analyzed by 3–8% gradient SDS-PAGE under reducing conditions followed by Western blot with anti-FLAG antibody. Migration of protein size markers is indicated in kDa on the *left* (*A* and *C*) or on the right (*B*). *EV*, empty vector; *NT*, no treatment; *T*, trimers.

gesting that further post-translational modifications occur during EMILIN-3 secretion.

A number of growth factors and other secreted proteins are thought to associate with the ECM because of their affinity for heparin and heparan sulfate proteoglycans (28, 29). Therefore, we investigated the possibility that EMILIN-3 might be endowed with heparin binding properties. Toward this aim, soluble heparin was added to the culture medium of transfected HEK293T cells. Whereas little or no EMILIN-3 was present in the conditioned media of cells grown under standard conditions, the protein could be readily detected in the medium fraction when transfected cells were grown in the presence of 50 μg/ml soluble heparin (Fig. 8*A*). To evaluate whether this effect was specific for heparin, we treated transfected HEK293T cells with the same concentrations of soluble chondroitin 4-sulfate and hyaluronic acid and analyzed the amount of EMILIN-3 released in the conditioned media. Although EMILIN-3 was abundant in heparin-treated medium, almost no protein was detected in media treated with the other glycosaminoglycans (Fig. 8*B*). Several potential interpretations can be put forward for these results including the possibility that soluble heparin in the medium may compete with the binding of EMILIN-3 to the ECM or that EMILIN-3 could bind directly to the heparin moiety. To investigate whether EMILIN-3 binds heparin, lysates of cells transfected with EMILIN-3L and -3S constructs were incubated with heparin-conjugated agarose beads, and the material bound to the beads was eluted with buffers at different salt concentrations and analyzed by Western blot. EMILIN-3L displayed efficient binding to the heparin-conjugated beads, and most of the protein eluted at high salt (0.6–1.0 M NaCl) concentrations. This association was specifically dependent on the heparin moiety because EMILIN-3L did not bind to unconjugated agarose beads (Fig. 8*C*). Similar results were also obtained for EMILIN-3S. To determine which fragment of EMILIN-3 is required for heparin binding, cells were transfected with the EMILIN-3ΔEMI construct. Interestingly, the EMILIN-3ΔEMI recombinant protein did not bind to heparin-conjugated beads, suggesting that the presence of the EMI domain is necessary for the association with heparin (Fig. 8*C*). In agreement with this, the EMILIN-3ΔEMI protein could be

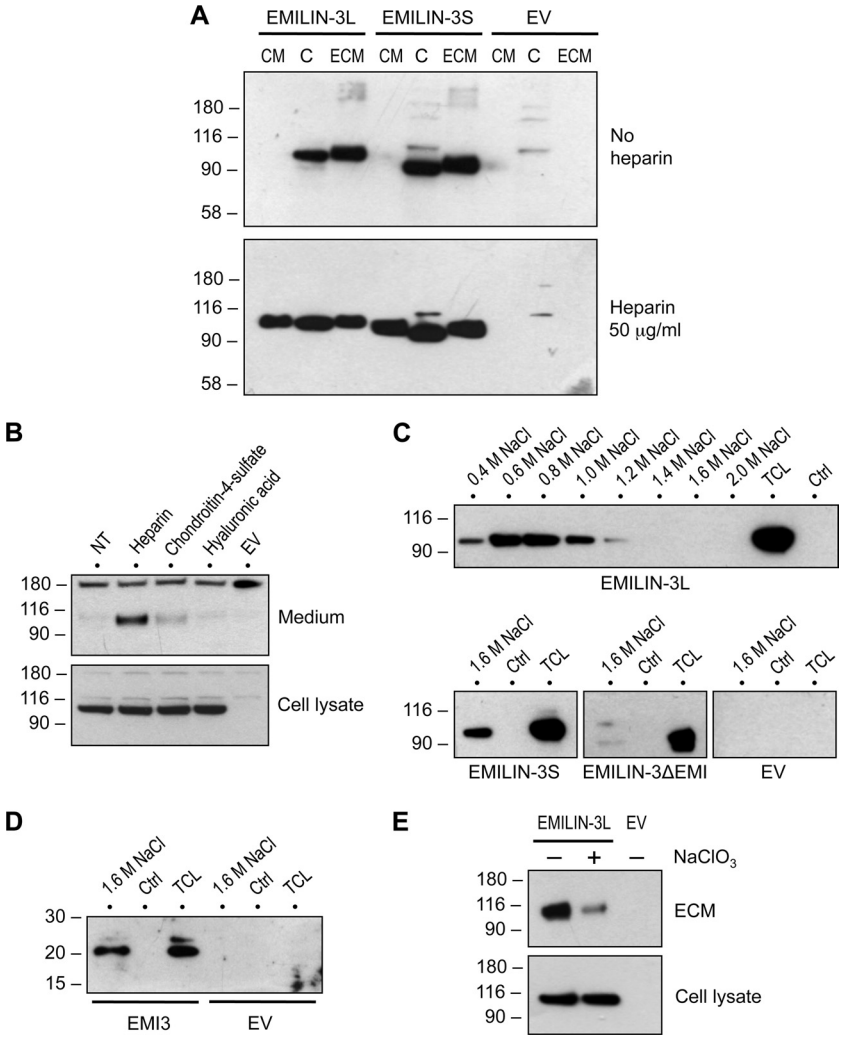

FIGURE 8. **EMILIN-3 is associated with ECM and binds to heparin.** *A*, after transfection with the indicated constructs, HEK293T cells were cultured in the absence or presence of 50 μg/ml soluble heparin. Cells were lysed at 4 °C in RIPA buffer, and the ECM material remaining on the culture dishes was extracted in Laemmli sample buffer at 90 °C. Cell lysate, conditioned medium, and ECM extract were analyzed by 4–12% gradient SDS-PAGE under reducing conditions followed by Western blot with rabbit EMILIN-3 antiserum. *B*, HEK293T transfected with EMILIN-3L were treated with the indicated glycosaminoglycans at 50 μg/ml, and cell lysates and conditioned media were subjected to SDS-PAGE on a 4–12% gel under reducing conditions and immunoblotted for EMILIN-3. *C* and *D*, cell lysates from HEK293T cells transfected with the indicated constructs were precipitated with heparin-conjugated agarose beads. After extensive washes, bound proteins were eluted with buffers containing increasing concentrations of NaCl from 0.4 to 2.0 M and separated by 4–12% gradient SDS-PAGE under reducing conditions, and transfected proteins were detected by Western blot with rabbit EMILIN-3 antiserum (*C*) or anti-FLAG antibody (*D*). *E*, HEK293T cells transfected with EMILIN-3L were left untreated (−) or treated with 30 μM sodium chlorate (+), and cell lysate and ECM extracts were prepared as above and analyzed by Western blot with rabbit EMILIN-3 antiserum. Migration of protein size markers is indicated in kDa on the *left* of each panel. *C*, cell layer; *CM*, conditioned medium; *Ctrl*, samples precipitated with unconjugated beads; *ECM*, insoluble ECM extract; *EV*, empty vector; *NT*, no treatment; *TCL*, total cell lysate.

readily detected in the conditioned medium of transfected cells (supplemental Fig. S8C).

To directly verify that the EMI domain is the heparin binding region of EMILIN-3, we prepared an expression construct (hereafter referred to as EMI3) encompassing the EMI domain and including amino acids 1–190 of EMILIN-3 with a FLAG tag at the C terminus. We then transfected HEK293T cells with the EMI3 construct and incubated the cell lysate with heparin-conjugated beads. In agreement with the above data, the recombinant EMI3 fragment did not bind to unconjugated beads but was efficiently precipitated by the heparin-conjugated beads, thus demonstrating that the EMI domain is directly responsible for the heparin binding properties of EMILIN-3 (Fig. 8*D*). To assess whether the strong association of EMILIN-3 to the ECM was mediated at least in part by the binding to endogenous heparan sulfate groups, we treated transfected HEK293T cells with the sulfotransferase inhibitor sodium chlorate and analyzed the insoluble ECM fraction. Interestingly, treatment with sodium chlorate strongly decreased the amount of transfected EMILIN-3 that could be extracted from the ECM, thus confirming that sulfated glycosaminoglycans markedly contribute to the association of EMILIN-3 with ECM (Fig. 8*E*).

EMILIN-3 Acts in Vitro as Pro-TGF-β Antagonist—A previous study demonstrated that EMILIN-1 is an extracellular antagonist of TGF-β signaling (10). To investigate whether EMILIN-3 has a similar function, we used the CAGA12-lux reporter plasmid as a direct readout for TGF-β activity. Initially, we transfected HEK293T cells with the reporter plasmid either in the presence or absence of the EMILIN-3L construct and treated the transfected cells with mature TGF-β1. In these

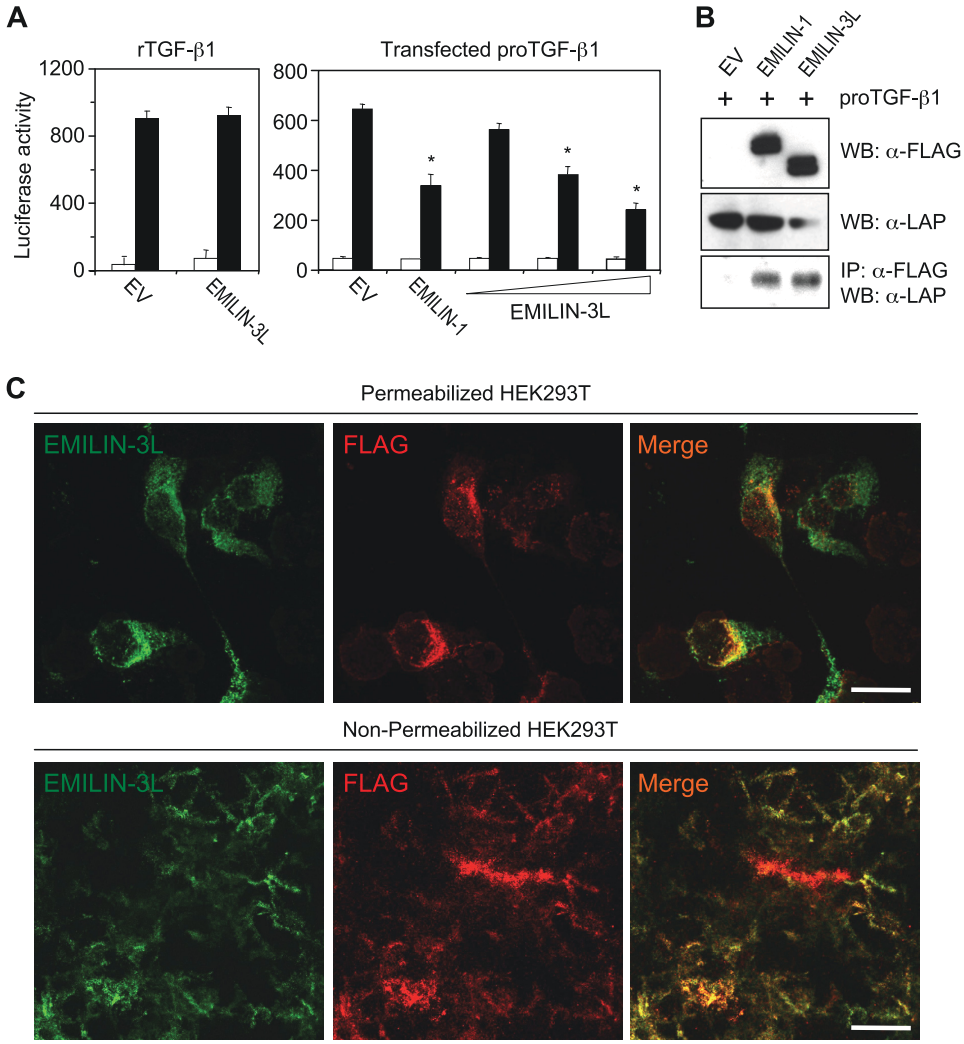

FIGURE 9. **EMILIN-3 is pro-TGF-β antagonist in HEK293T cells.** *A*, HEK293T cells were transfected in 24-well plates with the CAGA12-lux reporter plasmid (100 ng) alone or in combination with EMILIN-1 and EMILIN-3L expression constructs (300 ng). Transfected cells were left untreated (*open bars*) or treated overnight with 2.5 ng of recombinant mature human TGF-β1 (*rTGF-β1*) (*left panel*). Alternatively, cells were cotransfected with EMILIN-1 (300 ng), EMILIN-3 (100, 200, or 300 ng), and pro-TGF-β1 (C223S/C225S) variant plasmid (40 ng) (*right panel*). Luciferase activity was measured 24 h after the transfection. Data are shown as mean ± S.D. of at least three independent replicates. *, $p < 0.05$ compared with control (empty vector). *B*, HEK293T cells were transfected in 6-well plates with a pro-TGF-β1 expression plasmid (200 ng) together with FLAG-EMILIN-1, FLAG-EMILIN-3, or the empty vector (all 1 μg). The cell lysates were then subjected to immunoprecipitation with anti-FLAG antibody and Western blot with anti-latency-associated peptide (*LAP*) antibody. *C*, HEK293T were transfected with EMILIN-3L and a FLAG-tagged pro-TGF-β1 plasmid. Cells were then processed for immunofluorescence with or without permeabilization using rabbit EMILIN-3 antiserum and anti-FLAG antibody. For intracellular labeling, cells were permeabilized in methanol for 3 min at 20 °C. *Scale bar*, 25 (*upper panels*) or 50 μm (*lower panels*). *EV*, empty vector; *IP*, immunoprecipitation; *WB*, Western blot.

experimental conditions, EMILIN-3 had no effect on the luciferase reporter signal (Fig. 9*A*). We then tested the system by transfecting cells with a plasmid coding for the bioactive pro-TGF-β1 (C223S/C225S), a variant recombinant form that ensures that TGF-β1 is secreted as a biologically active molecule (30). We also used the EMILIN-1 construct as a positive control. When we cotransfected this pro-TGF-β1 plasmid with EMILIN-1 or with increasing concentrations of EMILIN-3, we detected a strong and dose-dependent inhibition of the reporter signal (Fig. 9*A*). Immunoprecipitation experiments on cell lysates of transfected HEK293T cells showed that pro-TGF-β1 was coprecipitated by both EMILIN-1 and EMILIN-3 (Fig. 9*B*). Further evidence for the interaction of EMILIN-3 with TGF-β1 was obtained upon subcellular colocalization by immunofluorescence. HEK293T cells were plated onto glass coverslips and cotransfected with the EMILIN-3L construct and a plasmid coding for pro-TGF-β1 with a FLAG tag inserted in the sequence of the mature cytokine (10). Under permeabilizing conditions, EMILIN-3 and pro-TGF-β1 colocalized in the endoplasmic reticulum compartment. Under non-permeabilizing conditions, the two proteins also partially colocalized in the ECM (Fig. 9*C*).

Next, we assessed whether EMILIN-3 could inhibit pro-TGF-β2 and -β3 activity as well. Toward this aim, we transfected cells with plasmids coding for the constitutively active forms of murine pro-TGF-β2 (C226S/C228S/C229S) and pro-TGF-β3 (C228S/C230S). Using a setup similar to that described above, we found that both EMILIN-3 and EMILIN-1 are very effective in inhibiting the signal induced by these two ligands (Fig. 10, *A* and *B*). It has been shown that EMILIN-1 can inhibit the pro-TGF-β-mediated signaling in the extracellular space through its EMI domain (10). To evaluate whether EMILIN-3

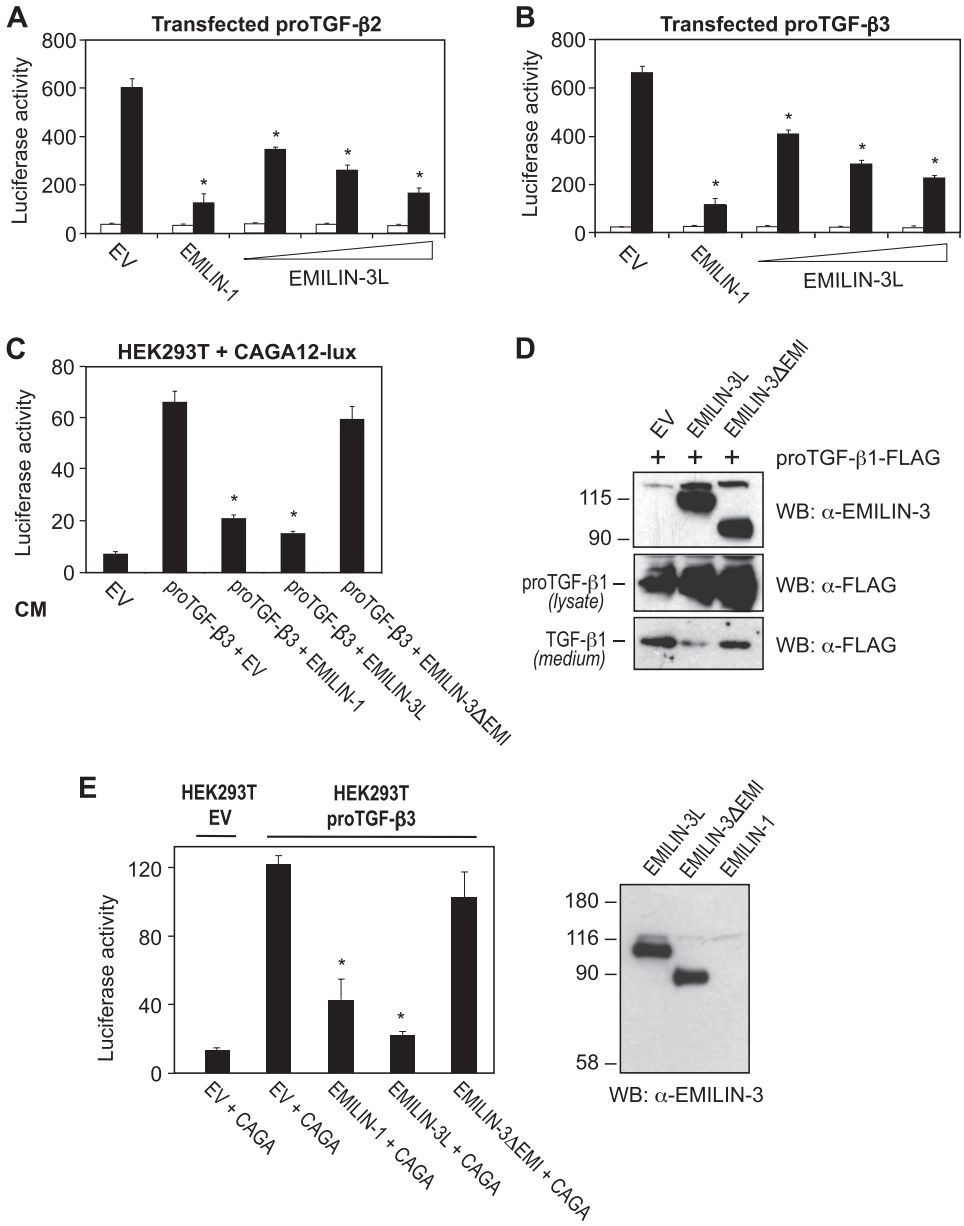

FIGURE 10. **EMILIN-3 is active in inhibiting pro-TGF-β2 and pro-TGF-β3 non-cell autonomously.** *A* and *B*, HEK293T cells were cotransfected with the CAGA12-lux reporter plasmid with plasmids coding for mutated bioactive forms of pro-TGF-β2 (*A*) or pro-TGF-β3 (*B*) and with EMILIN-1 (300 ng) or EMILIN-3L (100, 200, or 300 ng) expression constructs. Luciferase activity was measured 24 h after the transfection. Data are shown as mean ± S.D. of at least three independent replicates. *, $p < 0.05$ compared with control (empty vector). *C*, plasmid coding for the mutated bioactive pro-TGF-β3 (200 ng) was cotransfected with EMILIN-1, EMILIN-3L, or EMILIN-3ΔEMI expression constructs (all 2 μg) in a 6-well plate. After 48 h, the conditioned media were collected and used to treat HEK293T cells transfected with the CAGA12-lux reporter plasmid. Luciferase activity was measured 24 h after the treatment. Data are shown as mean ± S.D. of at least three independent replicates. *, $p < 0.05$ compared with control (empty vector). *D*, HEK293T cells were transfected with the indicated plasmids. Cell lysates and conditioned media were separated by 4–12% gradient SDS-PAGE under reducing conditions and immunoblotted with rabbit EMILIN-3 antiserum and anti-FLAG antibody. *E*, HEK293T cells were cotransfected with the CAGA12-lux reporter plasmid and the indicated expression constructs. Transfected cells were then mixed with cells transfected with the empty vector (*HEK293T EV*) or with the mutated bioactive pro-TGF-β3 plasmid (*HEK293T pro-TGF-β3*). After 24 h, mixed cells were lysed, and luciferase activity was measured (*left panel*). EMILIN-3 protein levels in the transfected cell lysates were assessed by Western blot with rabbit EMILIN-3 antiserum. Data are shown as mean ± S.D. of at least three independent replicates. *, $p < 0.05$ compared with control (empty vector). *CAGA*, CAGA12-lux; *CM*, conditioned medium; *EV*, empty vector; *WB*, Western blot.

can also act non-cell autonomously via its EMI domain, we carried out different experiments. First, we transfected pro-TGF-β3 alone or together with EMILIN constructs and then used the corresponding conditioned media to treat CAGA12-lux-transfected HEK293T cells. Strikingly, EMILIN-3L was able to inhibit almost completely the induction of the reporter plasmid, whereas EMILIN-3ΔEMI was much less efficient (Fig. 10*C*). In agreement with this, cotransfection of the FLAG-tagged pro-TGF-β1 with EMILIN-3 constructs showed that EMILIN-3L could prevent the release of the mature cytokine in the conditioned medium, whereas EMILIN-3ΔEMI could not (Fig. 10*D*). Finally, we performed cell mixing experiments to verify whether EMILIN-3 can act as a negative regulator of TGF-β signaling in the extracellular environment. Toward this aim, we prepared "responding" HEK293T cells transfected with the CAGA12-lux reporter plasmid in the presence or absence of

EMILIN constructs and "stimulatory" cells producing pro-TGF-β3. As expected, only when responding cells were mixed with stimulatory cells, the luciferase signal was induced. Remarkably, transfection of either EMILIN-1 or EMILIN-3 in responding cells led to a strong inhibition of the TGF-β response, whereas EMILIN-3ΔEMI was ineffective (Fig. 10*E*). Altogether, these latter sets of *in vitro* data indicate that EMILIN-3 works as an extracellular regulator of TGF-β signaling through its EMI domain.

DISCUSSION

Our data represent the first thorough characterization of the expression and biochemical properties of EMILIN-3. Two major features make EMILIN-3 a peculiar member within the EMILIN/Multimerin family of secreted proteins. First, as revealed by data presented in this work for the mouse and by our previous studies in zebrafish (15), EMILIN-3 is not expressed in any region of the cardiovascular system where all the other EMILINs/Multimerins are abundant. Second, despite a high degree of conservation of global protein organization with the other EMILINs/Multimerins (*i.e.* the presence of one EMI domain at the N-terminal end and a large region with high propensity for forming coiled coil structures), EMILIN-3 is lacking the C-terminal gC1q domain that is present in all other members of the family (2).

Our *in situ* hybridization data show that during mouse development EMILIN-3 has a dynamic pattern of expression, which only partially overlaps with the expression patterns of other EMILIN/Multimerin genes (2, 14). Expression of EMILIN-3 is first detected at E8.5–E.9.5 in the tail bud region, a structure known to contain a multipotent stem cell population (31). This peculiar expression during early embryogenesis was never observed for other EMILIN/Multimerin genes and is in full agreement with what we observed in early zebrafish embryos for EMILIN-3 ortholog genes (15). Subsequently and similar to EMILIN-1 (14), expression of EMILIN-3 becomes prominent in mesenchymal condensations where differentiation is taking place, such as branchial arches and limb buds. As the development proceeds, EMILIN-3 becomes restricted to more specific sites or disappears. For instance, EMILIN-3 is strongly expressed in the skeletal primordia, but when differentiation proceeds, the expression becomes confined to the perichondrium. The conspicuous expression of EMILIN-3 in the developing mouse skeleton is in agreement with previous reports (7) and with our studies in zebrafish where expression of EMILIN-3 orthologs was found in the cartilage primordia of the developing craniofacial skeleton (15). In another example, at early developmental stages, EMILIN-3 is strongly expressed in the esophageal buds, whereas at later stages, the expression is confined to myenteric cells. A further example is the central nervous system where EMILIN-3 is transiently expressed from E10.5 to E12.5 at the level of the ventricular zone midbrain where neuronal differentiation takes place (32). Interestingly, besides EMILIN-3, thus far only EMILIN-2 among the EMILIN/Multimerin proteins was found to be expressed in the nervous system (2). As reported for other EMILIN genes, during postnatal life, the levels of EMILIN-3 transcripts in different organs decrease with age, and in the adult, only a few tissues still express the mRNA. Immunofluorescence of adult tissues confirmed that EMILIN-3 has a restricted protein distribution, which does not overlap with that of any other EMILIN/Multimerin protein. As stated above, the most remarkable difference between EMILIN-3 and the other members of the EMILIN/Multimerin family is its absence from the cardiovascular system. Indeed, no mRNA expression was found throughout the development in blood vessels, heart, or kidneys, and no EMILIN-3 could be detected in these tissues even in adult mice.

As noted above, EMILIN-3 is the only protein of the EMILIN/Multimerin family that lacks the C-terminal gC1q domain. Because it has been proposed that this domain is involved in multimeric assembly of EMILIN-1 (11), the finding that EMILIN-3 exists *in vivo* as high molecular weight aggregates was unexpected. Further biochemical studies on transfected cells confirmed that EMILIN-3 is able to form disulfide-linked oligomers as reported previously for EMILIN-1, Multimerin-1, and Multimerin-2 (5, 11, 13, 33) and for the more distantly related Emu1 and Emu2 proteins (7). Our data indicate that the smallest EMILIN-3 oligomers have a mobility consistent with homotrimer formation and that EMILIN-3 predominantly exists as higher order oligomers. Transfection experiments with deletion constructs indicate that neither the gC1q domain nor the EMI domain is strictly necessary for the assembly of EMILIN-3, thus suggesting that the coiled coil regions with their flanking cysteine residues must be important for this process. Indeed, when the EMILIN-3CTR fragment corresponding to these regions was generated, it could be shown that this polypeptide formed disulfide bond-stabilized trimers with a substantial α-helical content. On the other hand, we found that EMILIN-1 is able to form higher order oligomers in the absence of the gC1q domain, but the process is impaired when the EMI domain is lacking, suggesting that the cysteine residues of the EMI domain contribute to the higher order self-assembly of EMILIN-1 and EMILIN-3. Although we did not investigate in detail which specific cysteines are required for EMILIN-3 self-assembly, the finding that EMILIN-3ΔEMI is able to associate with the full-length protein implies that the coiled coil regions are mediating this process.

Our biochemical studies on EMILIN-3 revealed another interesting property of this protein. We found that EMILIN-3 binds heparin with high affinity and that this binding is mediated by the EMI domain. It is not known whether other EMILINs/Multimerins or other EMI domains may have the same property, but the observation that Emu1 and Emu2 proteins are not detected in the conditioned medium of transfected cells (7) suggests that these two proteins may bind heparin as well. The cysteine-rich EMI domain was already found to work as a self-interacting module (9) and as a protein-protein interaction domain as in the case of the binding to pro-TGFβ-1 (10). Our results reveal a new function of the EMI domain that may be responsible for the interaction of EMILIN-3 with the heparan sulfate moiety of specific ECM and cell surface proteoglycans, such as perlecan, syndecans, and glypican, and/or secreted growth factors. Protein binding to heparin usually requires clusters of basic amino acid residues interspersed with one or two non-basic amino acid residues in the protein sequence (34). Although no typical heparin-binding consensus

sequences are found in EMILIN-3, our data clearly indicate that the EMI domain alone is sufficient to bind heparin. Notably, among the extracellular proteins known to bind heparin/heparan sulfate chains, there are several elastic fiber-associated proteins, such as tropoelastin (35), fibrillin-1 (36), latent TGF-β binding proteins (37, 38), and various members of the TGF-β superfamily (39).

TGF-β ligands are usually secreted as large latent complexes covalently bound to latent TGF-β-binding proteins and incorporated into the ECM in association with microfibrils (40). Although it is not known yet whether EMILIN-3, like EMILIN-1 (1), associates with elastic fiber components, our data indicate that EMILIN-3 could participate in the extracellular regulation of the bioavailability of TGF-β ligands. In our assays, EMILIN-3 appears ineffective in inhibiting the activity of the mature cytokine, whereas it is very effective in inhibiting the activity of pro-TGF-β1 as well as pro-TGF-β2 and -β3. Interestingly, our *in vitro* luciferase assay experiments showed that EMILIN-1 has a similar inhibitory activity for all three pro-TGF-β molecules, a function that was previously investigated only for pro-TGF-β1 (10). Although this activity largely relies upon the EMI domain, the precise molecular mechanisms involved in the *in vivo* regulation of TGF-β activity by EMILIN proteins remain to be understood. In this respect, it will be interesting to investigate whether EMILIN proteins contribute to the regulation of the bioavailability of mature TGF-β ligands by also interacting with the large ECM functional complex composed by latent TGF-β-binding proteins, fibrillin-1 and -2, and other microfibril-associated proteins, such as MAGP-1 and fibulin-4 (40, 41). Moreover, the finding that EMILIN-3 binds heparin suggests that this protein may participate in the modulation in the extracellular space of the availability and distribution of other secreted factors known to be regulated by heparan sulfate proteoglycans, such as Wnt, Hedgehog, or bone morphogenetic protein ligands (42).

Altogether, the data reported in this work represent the first detailed characterization of the distribution and biochemical properties of EMILIN-3. Given the unique primary structure and the peculiar expression of this member of the EMILIN/Multimerin family, future work aimed at elucidating its *in vivo* functional properties will allow a full understanding of the biological role of EMILIN-3 in embryonic development and tissue homeostasis.

Acknowledgments—We thank Birgit Kobbe for the generation of EMILIN-3 antibodies and Tullio Pozzan for the D1ER plasmid.

REFERENCES

1. Bressan, G. M., Daga-Gordini, D., Colombatti, A., Castellani, I., Marigo V, and Volpin, D. (1993) Emilin, a component of elastic fibers preferentially located at the elastin-microfibrils interface. *J. Cell Biol.* **121,** 201–212
2. Braghetta, P., Ferrari, A., De Gemmis, P., Zanetti, M., Volpin, D., Bonaldo, P., and Bressan, G. M. (2004) Overlapping, complementary and site-specific expression pattern of genes of the EMILIN/Multimerin family. *Matrix Biol.* **22,** 549–556
3. Hayward, C. P., Hassell, J. A., Denomme, G. A., Rachubinski, R. A., Brown, C., and Kelton, J. G. (1995) The cDNA sequence of human endothelial cell multimerin. A unique protein with RGDS, coiled-coil, and epidermal growth factor-like domains and a carboxyl terminus similar to the globular domain of complement C1q and collagens type VIII and X. *J. Biol. Chem.* **270,** 18246–18251
4. Doliana, R., Canton, A., Bucciotti, F., Mongiat, M., Bonaldo, P., and Colombatti, A. (2000) Structure, chromosomal localization, and promoter analysis of the human elastin microfibril interface located protein (EMILIN) gene. *J. Biol. Chem.* **275,** 785–792
5. Christian, S., Ahorn, H., Novatchkova, M., Garin-Chesa, P., Park, J. E., Weber, G., Eisenhaber, F., Rettig, W. J., and Lenter, M. C. (2001) Molecular cloning and characterization of EndoGlyx-1, an EMILIN-like multisubunit glycoprotein of vascular endothelium. *J. Biol. Chem.* **276,** 48588–48595
6. Doliana, R., Bot, S., Mungiguerra, G., Canton, A., Cilli, S. P., and Colombatti, A. (2001) Isolation and characterization of EMILIN-2, a new component of the growing EMILINs family and a member of the EMI domain-containing superfamily. *J. Biol. Chem.* **276,** 12003–12011
7. Leimeister, C., Steidl, C., Schumacher, N., Erhard, S., and Gessler, M. (2002) Developmental expression and biochemical characterization of Emu family members. *Dev. Biol.* **249,** 204–218
8. Doi, M., Nagano, A., and Nakamura, Y. (2004) Molecular cloning and characterization of a novel gene, EMILIN-5, and its possible involvement in skeletal development. *Biochem. Biophys. Res. Commun.* **313,** 888–893
9. Doliana, R., Bot, S., Bonaldo, P., and Colombatti, A. (2000) EMI, a novel cysteine-rich domain of EMILINs and other extracellular proteins, interacts with the gC1q domains and participates in multimerization. *FEBS Lett.* **484,** 164–168
10. Zacchigna, L., Vecchione, C., Notte, A., Cordenonsi, M., Dupont, S., Maretto, S., Cifelli, G., Ferrari, A., Maffei, A., Fabbro, C., Braghetta, P., Marino, G., Selvetella, G., Aretini, A., Colonnese, C., Bettarini, U., Russo, G., Soligo, S., Adorno, M., Bonaldo, P., Volpin, D., Piccolo, S., Lembo, G., and Bressan, G. M. (2006) Emilin1 links TGF-β maturation to blood pressure homeostasis. *Cell* **124,** 929–942
11. Mongiat, M., Mungiguerra, G., Bot, S., Mucignat, M. T., Giacomello, E., Doliana, R., and Colombatti, A. (2000) Self-assembly and supramolecular organization of EMILIN. *J. Biol. Chem.* **275,** 25471–25480
12. Spessotto, P., Cervi, M., Mucignat, M. T., Mungiguerra, G., Sartoretto, I., Doliana, R., and Colombatti, A. (2003) β1 integrin-dependent cell adhesion to EMILIN-1 is mediated by the gC1q domain. *J. Biol. Chem.* **278,** 6160–6167
13. Hayward, C. P., Warkentin, T. E., Horsewood, P., and Kelton, J. G. (1991) Multimerin: a series of large disulfide-linked multimeric proteins within platelets. *Blood* **77,** 2556–2560
14. Braghetta, P., Ferrari, A., de Gemmis, P., Zanetti, M., Volpin, D., Bonaldo, P., and Bressan, G. M. (2002) Expression of the EMILIN-1 gene during mouse development. *Matrix Biol.* **21,** 603–609
15. Milanetto, M., Tiso, N., Braghetta, P., Volpin, D., Argenton, F., and Bonaldo, P. (2008) Emilin genes are duplicated and dynamically expressed during zebrafish embryonic development. *Dev. Dyn.* **237,** 222–232
16. Zanetti, M., Braghetta, P., Sabatelli, P., Mura, I., Doliana, R., Colombatti, A., Volpin, D., Bonaldo, P., and Bressan, G. M. (2004) EMILIN-1 deficiency induces elastogenesis and vascular cell defects. *Mol. Cell. Biol.* **24,** 638–650
17. Danussi, C., Spessotto, P., Petrucco, A., Wassermann, B., Sabatelli, P., Montesi, M., Doliana, R., Bressan, G. M., and Colombatti, A. (2008) Emilin1 deficiency causes structural and functional defects of lymphatic vasculature. *Mol. Cell. Biol.* **28,** 4026–4039
18. Danussi, C., Petrucco, A., Wassermann, B., Pivetta, E., Modica, T. M., Belluz Ldel, B., Colombatti, A., and Spessotto, P. (2011) EMILIN1-α4/α9 integrin interaction inhibits dermal fibroblast and keratinocyte proliferation. *J. Cell Biol.* **195,** 131–145
19. Mongiat, M., Ligresti, G., Marastoni, S., Lorenzon, E., Doliana, R., and Colombatti, A. (2007) Regulation of the extrinsic apoptotic pathway by the extracellular matrix glycoprotein EMILIN2. *Mol. Cell. Biol.* **27,** 7176–7187
20. Kohfeldt, E., Maurer, P., Vannahme, C., and Timpl, R. (1997) Properties of the extracellular calcium binding module of the proteoglycan testican.

FEBS Lett. **414,** 557–561
21. Larraín, J., Bachiller, D., Lu, B., Agius, E., Piccolo, S., and De Robertis, E. M. (2000) BMP-binding modules in chordin: a model for signalling regulation in the extracellular space. *Development* **127,** 821–830
22. Sambrook, J., and Russell, D. W. (2001) *Molecular Cloning: A Laboratory Manual*, 3rd Ed., pp. 16.1–16.28, Cold Spring Harbor Laboratory Press, Cold Spring Harbor, NY
23. Whitmore, L., and Wallace, B. A. (2004) DICHROWEB, an online server for protein secondary structure analyses from circular dichroism spectroscopic data. *Nucleic Acids Res.* **32,** W668–W673
24. Andrade, M. A., Chacón, P., Merelo, J. J., and Morán, F. (1993) Evaluation of secondary structure of proteins from UV circular dichroism spectra using an unsupervised learning neural network. *Protein Eng.* **6,** 383–390
25. Lupas, A., Van Dyke, M., and Stock, J. (1991) Predicting coiled coils from protein sequences. *Science* **252,** 1162–1164
26. Hodges, R. S., Zhou, N. E., Kay, C. M., and Semchuk, P. D. (1990) Synthetic model proteins: contribution of hydrophobic residues and disulfide bonds to protein stability. *Pept. Res.* **3,** 123–137
27. Greenfield, N. J., and Hitchcock-DeGregori, S. E. (1993) Conformational intermediates in the folding of a coiled-coil model peptide of the N-terminus of tropomyosin and α α-tropomyosin. *Protein Sci.* **2,** 1263–1273
28. Bernfield, M., Götte, M., Park, P. W., Reizes, O., Fitzgerald, M. L., Lincecum, J., and Zako, M. (1999) Functions of cell surface heparan sulfate proteoglycans. *Annu. Rev. Biochem.* **68,** 729–777
29. Lin, X. (2004) Functions of heparan sulfate proteoglycans in cell signaling during development. *Development* **131,** 6009–60021
30. Brunner, A. M., Marquardt, H., Malacko, A. R., Lioubin, M. N., and Purchio, A. F. (1989) Site-directed mutagenesis of cysteine residues in the pro region of the transforming growth factor β1 precursor. Expression and characterization of mutant proteins. *J. Biol. Chem.* **264,** 13660–13664
31. Wilson, V., Olivera-Martinez, I., and Storey, K. G. (2009) Stem cells, signals and vertebrate body axis extension. *Development* **136,** 1591–1604
32. Corbin, J. G., Gaiano, N., Juliano, S. L., Poluch, S., Stancik, E., and Haydar, T. F. (2008) Regulation of neural progenitor cell development in the nervous system. *J. Neurochem.* **106,** 2272–2287
33. Colombatti, A., Bonaldo, P., Volpin, D., and Bressan, G. M. (1988) The elastin associated glycoprotein gp115. Synthesis and secretion by chick cells in culture. *J. Biol. Chem.* **263,** 17534–17540
34. Fromm, J. R., Hileman, R. E., Caldwell, E. E., Weiler, J. M., and Linhardt, R. J. (1997) Pattern and spacing of basic amino acids in heparin binding sites. *Arch. Biochem. Biophys.* **343,** 92–100
35. Broekelmann, T. J., Kozel, B. A., Ishibashi, H., Werneck, C. C., Keeley, F. W., Zhang, L., and Mecham, R. P. (2005) Tropoelastin interacts with cell-surface glycosaminoglycans via its COOH-terminal domain. *J. Biol. Chem.* **280,** 40939–40947
36. Cain, S. A., Baldock, C., Gallagher, J., Morgan, A., Bax, D. V., Weiss, A. S., Shuttleworth, C. A., and Kielty, C. M. (2005) Fibrillin-1 interactions with heparin. Implications for microfibril and elastic fiber assembly. *J. Biol. Chem.* **280,** 30526–30537
37. Kantola, A. K., Keski-Oja, J., and Koli, K. (2008) Fibronectin and heparin binding domains of latent TGF-β binding protein (LTBP)-4 mediate matrix targeting and cell adhesion. *Exp. Cell Res.* **314,** 2488–2500
38. Parsi, M. K., Adams, J. R., Whitelock, J., and Gibson, M. A. (2010) LTBP-2 has multiple heparin/heparan sulfate binding sites. *Matrix Biol.* **29,** 393–401
39. Rider, C. C. (2006) Heparin/heparan sulphate binding in the TGF-β cytokine superfamily. *Biochem. Soc. Trans.* **34,** 458–460
40. Annes, J. P., Munger, J. S., and Rifkin, D. B. (2003) Making sense of latent TGFβ activation. *J. Cell Sci.* **116,** 217–224
41. Massam-Wu, T., Chiu, M., Choudhury, R., Chaudhry, S. S., Baldwin, A. K., McGovern, A., Baldock, C., Shuttleworth, C. A., and Kielty, C. M. (2010) Assembly of fibrillin microfibrils governs extracellular deposition of latent TGFβ. *J. Cell Sci.* **123,** 3006–3018
42. Häcker, U., Nybakken, K., and Perrimon, N. (2005) Heparan sulphate proteoglycans: the sweet side of development. *Nat. Rev. Mol. Cell Biol.* **6,** 530–541